

RESEARCH ARTICLE

10.1029/2017JF004395

Key Points:

- Elevation change and flux divergence enable the calibration and validation of debris thickness estimates for debris-covered glaciers
- Surface lowering associated with ice cliffs and supraglacial ponds significantly reduces estimates of thick debris
- Thermal conductivity and elevation change errors contribute the most to uncertainty associated with debris thickness estimates

Supporting Information:

- Supporting Information S1

Correspondence to:

D. R. Rounce,
david.rounce@utexas.edu

Citation:

Rounce, D. R., King, O., McCarthy, M., Shean, D. E., & Salerno, F. (2018). Quantifying debris thickness of debris-covered glaciers in the Everest region of Nepal through inversion of a subdebris melt model. *Journal of Geophysical Research: Earth Surface*, 123, 1094–1115. <https://doi.org/10.1029/2017JF004395>

Received 10 JUN 2017

Accepted 2 APR 2018

Accepted article online 25 APR 2018

Published online 22 MAY 2018

Quantifying Debris Thickness of Debris-Covered Glaciers in the Everest Region of Nepal Through Inversion of a Subdebris Melt Model

David R. Rounce^{1,2} , Owen King³, Michael McCarthy^{4,5}, David E. Shean⁶ , and Franco Salerno⁷ 

¹Center for Research in Water Resources, University of Texas at Austin, Austin, TX, USA, ²Geophysical Institute, University of Alaska Fairbanks, Fairbanks, AK, USA, ³School of Geography, University of Leeds, Leeds, UK, ⁴British Antarctic Survey, Natural Environment Research Council, Cambridge, UK, ⁵Scott Polar Research Institute, University of Cambridge, Cambridge, UK, ⁶Polar Science Center, Applied Physics Lab, University of Washington, Seattle, WA, USA, ⁷National Research Council, Water Research Institute, Brugherio, Italy

Abstract Debris-covered glaciers are ubiquitous in the Himalaya, and supraglacial debris significantly alters how glaciers respond to climate forcing. Estimating debris thickness at the glacier scale, however, remains a challenge. This study inverts a subdebris melt model to estimate debris thickness for three glaciers in the Everest region from digital elevation model difference-derived elevation change. Flux divergences are estimated from ice thickness and surface velocity data. Monte Carlo simulations are used to incorporate the uncertainties associated with debris properties, flux divergence, and elevation change. On Ngozumpa Glacier, surface lowering data from 2010 to 2012 and 2012 to 2014 are used to calibrate and validate the method, respectively. The debris thickness estimates are consistent with existing in situ measurements. The method performs well over both actively flowing and stagnant parts of the glacier and is able to accurately estimate thicker debris (>0.5 m). Uncertainties associated with the thermal conductivity and elevation change contribute the most to uncertainties of the debris thickness estimates. The surface lowering associated with ice cliffs and supraglacial ponds was found to significantly reduce debris thickness, especially for thicker debris. The method is also applied to Khumbu and Imja-Lhotse Shar Glaciers to highlight its potential for regional application.

Plain Language Summary Debris-covered glaciers are ubiquitous in the Himalaya, and this debris significantly alters the evolution of these glaciers. Estimating the thickness of debris on these glaciers, however, remains a challenge. This study develops a novel method for estimating the debris thickness on three glaciers in the Everest region of Nepal based on digital elevation models, surface velocity data, ice thickness estimates, and a debris-covered glacier energy balance model. The method was calibrated and validated on Ngozumpa Glacier, one of the largest debris-covered glaciers in Nepal, and was found to accurately estimate debris thickness. Specifically, this method was able to estimate thick debris (>0.5 m), which has been a major limitation of previous studies. This is important because thick debris significantly reduces glacier melt rates by insulating the underlying ice. This study creates a step-change in our ability to model the past, present, and future evolution of debris-covered glaciers.

1. Introduction

Glaciers in the Himalaya are an important resource as they provide water for drinking, agriculture, sanitation, and hydropower to more than 800 million people (Bolch et al., 2012; Pritchard, 2017). The rapid melting of Himalayan glaciers in response to climate change is already altering water availability, with estimates projecting severe water shortages by 2050 (Immerzeel et al., 2010; Soncini et al., 2016). Approximately 14–18% of total glacier area in the Himalaya is debris covered (Kääb et al., 2012). Some areas (e.g., the south sloping glaciers in the Everest region) currently have upward of 32% debris coverage, which has increased by $18 \pm 3\%$ since 1962 (Thakuri et al., 2014).

Supraglacial debris thickness significantly alters how glaciers respond to climate forcing. A thin layer of debris (less than several centimeters) enhances melt, while a thick layer of debris insulates the underlying ice and reduces melt (Nicholson & Benn, 2006; Østrem, 1959). In the Everest region, debris thickness may be up to several meters thick (Nicholson & Benn, 2012; Rounce & McKinney, 2014). However, while the relationship

between debris thickness and melt is well known (commonly shown on the Østrem Curve; Østrem, 1959), quantifying debris thickness at the glacier scale is still a major challenge.

In the Everest region, studies have documented long-term and apparent accelerating mass loss from debris-covered glaciers using a geodetic approach. From the 1970s to the present, mass balance has been estimated to range from -0.32 ± 0.08 to -0.52 ± 0.22 meters water equivalent per year (Bolch et al., 2011; Gardelle et al., 2013; King et al., 2017; Nuimura et al., 2012). Projecting glacier change into the future has proven more challenging, largely due to uncertainties related to the effects of debris cover. This is highlighted by recent studies, which estimate glacier volume loss could range from 8% to 95% compared to present-day total volume (Rowan et al., 2015; Shea et al., 2015; Soncini et al., 2016). Clearly, the mechanisms and ablation processes driving ice loss over debris-covered glaciers need to be better understood to allow for the accurate prediction of glacier change in the future.

In situ debris thickness measurements have been made by manual excavation (Patel et al., 2016; Reid et al., 2012; Rounce & McKinney, 2014; Soncini et al., 2016), surveying debris above exposed ice faces using a total station and reflector (Nicholson & Benn, 2012) or terrestrial photography (Nicholson & Mertes, 2017), and ground penetrating radar (McCarthy et al., 2017; Nicholson & Mertes, 2017; Wu & Liu, 2012). These methods are difficult to apply at mountain-range (or even glacier) scale due to time and labor constraints, and measurements are therefore scarce. When available, measurements are often focused on localized sections of a glacier and may not be representative of the entire glacier.

Recent studies attempt to derive debris thickness from satellite imagery by combining surface temperature estimates with surface energy balance models (Foster et al., 2012; Rounce & McKinney, 2014; Schauwecker et al., 2015), by defining empirical relationships between surface temperature and debris thickness (Mihalcea et al., 2008; Soncini et al., 2016), or by inverting the Østrem Curve using an energy balance model and surface lowering measurements (Ragetti et al., 2015). Uncertainties associated with meteorological data, debris properties, and components of the surface energy balance model are considerable obstacles to these approaches. For the thermal approaches, studies have highlighted the importance of properly accounting for the turbulent heat fluxes and nonlinear temperature gradient within the debris (Foster et al., 2012; Rounce & McKinney, 2014; Schauwecker et al., 2015) but have been unable to accurately estimate debris thicker than 0.5 m. Further issues arise from the low resolution of thermal imagery (60–100 m), which causes a “mixed pixel” effect, that is, when debris, ice cliffs, and/or supraglacial ponds exist in the same pixel thereby reducing the surface temperature and causing the thickness of debris to be underestimated. The Østrem inversion method used by Ragetti et al. (2015) yields promising results for debris thickness; however, validation of the modeled results is limited. Proper validation of model results is a general issue for remote sensing approaches in the Himalaya due to the lack of in situ measurements.

Debris-covered glacier energy balance models applied at sites with well-quantified inputs have been found to accurately reproduce measured surface temperatures and melt rates for a range of debris types and thicknesses (Collier et al., 2014; Evatt et al., 2015; Reid & Brock, 2010; Rounce et al., 2015). However, accounting for the spatial variation in surface properties and the role of moisture in the debris remains a challenge. The important debris properties include thickness, albedo, surface roughness, and thermal conductivity. In the Everest region, debris thickness ranges from bare ice to several meters (Nakawo et al., 1986; Nicholson & Benn, 2012; Nicholson & Mertes, 2017; Rounce & McKinney, 2014; Soncini et al., 2016), debris albedo ranges from 0.1 to 0.4 (Inoue & Yoshida, 1980; Kayastha et al., 2000; LeJeune et al., 2013; Nicholson & Benn, 2012), surface roughness from 0.0035 to 0.0600 m (Inoue & Yoshida, 1980; Quincey et al., 2017; Takeuchi et al., 2000), and thermal conductivity from 0.47 to 1.62 $\text{W m}^{-1} \text{K}^{-1}$ (Conway & Rasmussen, 2000; Nicholson & Benn, 2012; Rounce et al., 2015; Rounce & McKinney, 2014). Studies frequently assume a single value for these parameters over the entire glacier (e.g., Rounce & McKinney, 2014); however, each of these surface properties has large spatial and temporal variations, even on the same glacier (e.g., Conway & Rasmussen, 2000; Nicholson & Benn, 2012; Rounce et al., 2015).

This study develops a novel method of mapping debris thickness from subdebris melt rates based on elevation change and flux divergence. It uses a forward model of subdebris melting (Rounce et al., 2015) in an inverse approach, such that debris thickness is iteratively adjusted until the modeled subdebris melt rate agrees with the observed subdebris melt rate. Elevation change is quantified from a series of digital elevation models (DEMs), flux divergences are quantified from ice thickness and surface velocity data, and the

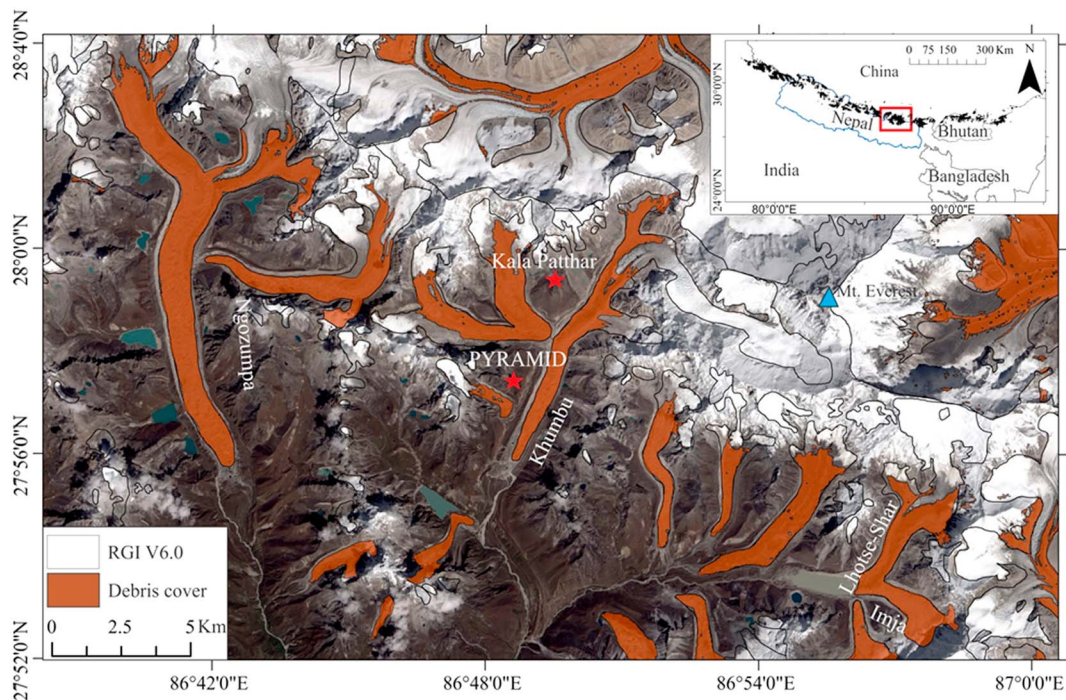


Figure 1. Study area showing debris cover extent on Ngozumpa, Khumbu, and Imja-Lhotse Shar Glaciers along with Pyramid Station and the Kala Patthar weather station (stars). Inset shows location within the Nepal Himalaya. Background image is Landsat 8 from 30 September 2015.

subdebris melt model is driven by meteorological data from a nearby weather station. Monte Carlo simulations incorporate the uncertainty associated with the debris properties, flux divergence, and elevation change into the debris thickness estimates. Surface lowering data from 2010 to 2012 are used to calibrate the debris thickness method over Ngozumpa Glacier, and surface lowering data from 2012 to 2014 are used for validation. The method is then applied to Khumbu and Imja-Lhotse Shar Glaciers using surface lowering data from 2009 to 2015. Modeled debris thicknesses from these three glaciers are compared to in situ measurements to further assess the performance of the method. Additionally, debris thickness is estimated from surface lowering rates that both include and exclude ice cliffs and supraglacial ponds to quantify their impact on reducing modeled debris thickness.

2. Study Area

This study focuses on three glaciers situated in the Dudh Koshi catchment of the Everest region: Ngozumpa, Khumbu, and Imja-Lhotse Shar Glaciers (Figure 1). Ngozumpa Glacier (27.931°N, 86.715°E) flows down the southeast face of Cho Oyu (8,188 m above sea level, a.s.l.) and the southwest face of Gyachung Kang (7,952 m a.s.l.). The glacier is 18-km long and terminates at 4,659 m a.s.l. (Thompson et al., 2016). The lower 15 km is almost entirely debris covered, and the glacier's low surface gradient further downglacier facilitates the development of numerous ice cliffs and supraglacial ponds (Salerno et al., 2017; Watson et al., 2016, 2017). Thompson et al. (2016) suggested that an active/inactive boundary exists approximately 6.5 km upstream of the glacier terminus, which agrees with the area Quincey et al. (2009) termed relatively stagnant (<10 m/a). Nicholson and Benn (2012) made observations of debris thickness that suggest a decrease upglacier, from a median of 1–1.5 m at 1 km from the terminus to less than 0.5 m at 7 km from the terminus.

Thompson et al. (2016) showed that although ice cliffs account for 39% of melting on the debris-covered area, the majority of melting (52%) occurs below the debris. Ngozumpa Glacier also has a complex englacial drainage system, which effects the evacuation of meltwater and spatial patterns of surface mass loss (Benn et al., 2017). The moraine-dammed lake at its terminus, commonly referred to as Spillway Lake, experienced rapid expansion after 2001 (Thompson et al., 2012), but has recently experienced a reduction in lake area that is thought to be temporary, as a result of local sediment redistribution on the surrounding slopes

(Thompson et al., 2016). Thakuri et al. (2014) reported a surface area loss of -1.4% from 1962 to 2011, and King et al. (2017) reported substantial surface lowering in the high-altitude clean-ice areas of the glacier from 2000 to 2014/2015.

Khumbu Glacier (27.932°N , 86.812°E , Figure 1) originates in the Western Cwm below Mount Everest (8,848 m a.s.l.) and terminates at 4,876 m a.s.l. The glacier is 15.7 km in length, covers an area of 26.5 km^2 , and has an ablation zone flanked by large moraines, built up during the Little Ice Age, that contribute to supraglacial debris. The low surface gradient of the tongue of the glacier has facilitated the development of an extensive ice cliff and supraglacial pond network that has expanded in the last 15 years (Salerno et al., 2017; Watson et al., 2016, 2017). Bolch et al. (2011) quantified the surface lowering rate of the entire debris covered ablation zone of Khumbu Glacier over multiple time periods between 1962 and 2007. They showed an increase in surface lowering over this period, which is concomitant with the 60% increase in debris cover since the 1960s shown by Thakuri et al. (2014). Surface velocities from 1992 to 2002 (Quincey et al., 2009) and 2013 to 2014 (Rowan et al., 2015) show that the lowermost portion of the glacier tongue has slowed down in recent years. Rowan et al. (2015) suggested that an active/inactive boundary exists 5.4 km upstream from the glacier terminus below which the glacier is relatively stagnant ($<10\text{ m/a}$) and above which the velocities range from 10 to 70 m/a. Nuimura et al. (2011) estimated the emergence velocity 7 km upstream from the terminus to be 5.06 m/a from 1995 to 2004.

Imja-Lhotse Shar Glacier (27.901°N , 86.938°E , Figure 1) refers to two avalanche-fed debris-covered glaciers that converge and terminate into Imja Tsho (Lake) at 5,000 m a.s.l. Debris cover extends roughly 3 and 4.5 km upstream of the calving front and covers an area of 1.5 and 4.7 km^2 for Imja and Lhotse Shar Glaciers, respectively. The thickness of this debris cover decreases upglacier (Rounce & McKinney, 2014), and the areal extent of debris cover has increased in recent years due to the glacier experiencing significant mass loss (Thakuri et al., 2016). Mass loss has occurred as a result of the rapid expansion of Imja Tsho (Thakuri et al., 2016), the melt beneath the debris cover (Rounce et al., 2015), and the melt associated with bare ice cliffs and supraglacial ponds (Watson et al., 2016). Glacier surface velocity has decreased since 1992 (Thakuri et al., 2016), although Lhotse Shar Glacier and the upper portion of Imja Glacier appear to remain active (Bolch et al., 2008; Thakuri et al., 2016).

3. Methods

3.1. DEM Generation and Elevation Change

Stereo-photogrammetric DEMs were generated using imagery acquired by three different optical sensors (Table 1). Four of the six DEMs were generated from WorldView-2 and GeoEye-1 imagery (DigitalGlobe, Inc.) using the Ames Stereo Pipeline (Shean, 2017a, 2017b; Shean et al., 2016). Two additional DEMs were generated using imagery from the Advanced Land Observing Satellite-Panchromatic Remote-Sensing Instrument for Stereo Mapping (ALOS-PRISM) archive and the Leica Photogrammetry Suite in ERDAS Imagine (2013; Table 1). Without suitable ground control points for the ALOS-PRISM DEM bundle adjustment, distinctive features found on stable, off-glacier terrain visible in both the ALOS-PRISM imagery and the high-resolution imagery available in Google Earth were matched ($n = 50$ and 46 for Khumbu and Imja-Lhotse Shar Glacier DEMs, respectively), and their associated spot heights were used in the DEM generation process. The source of elevation data from Google Earth varies by region based on data availability. Given the remote nature of the Everest region, the elevation data source here is likely the SRTM (Shuttle Radar Topography Mission) or ASTER (Advanced Spaceborne Thermal Emission and Reflection Radiometer), which have a vertical error around 10 m in this region (Farr et al., 2007; Fujita et al., 2008).

To prevent the production of erroneous difference data over glacier surfaces through the subtraction of DEMs with inconsistent geolocation, the methods of Nuth and Kääb (2011) were followed to coregister and detilt the DEMs. These methods are based on the relationship between elevation differences and the derivatives of slope and aspect of two misaligned DEMs. Only areas of DEMs that can be realistically assumed to have been stable over the time separating the acquisition dates of scenes were used to derive offset vectors. Of the three sensors, geolocation accuracy is poorest for ALOS-PRISM, so the ALOS-PRISM DEMs, used for Khumbu and Imja-Lhotse Shar Glaciers, were referenced to the WorldView-2 and GeoEye-1 DEMs, respectively, while for Ngozumpa Glacier the GeoEye-1 DEM from 2012 was used as the reference data set for coregistration.

Table 1
High-Resolution Satellite Imagery Used to Generate Digital Elevation Models

Glacier	Date of image	Sensor	Scene ID
Ngozumpa	9 Jun 2010	GeoEye-1	1050410001B4E300/1050410001B4DC00
	23 Dec 2012 ^a	GeoEye-1	1050410000E8C900/1050410000E0AE00
	18 Oct 2014	GeoEye-1	1050410011888400/1050410011888300
Khumbu	3 Mar 2009	ALOS-PRISM	ALPSMW16663040/ALPSMW166603095
	2 Feb 2015 ^a	WorldView-2	103001003D4C7900/103001003D7AFE00
Imja-Lhotse Shar	3 Mar 2009	ALOS-PRISM	ALPSMW16663040/ALPSMW166603095
	24 Jan 2015 ^a	GeoEye-1	1050410012196D00/1050410012196B00

^aDenote the master digital elevation model used for coregistration.

All DEM products were resampled to a common resolution of 10 m before computing elevation change. No elevation change versus elevation bias correction was necessary. The elevation change data sets were then filtered to remove any unrealistic changes due to artifacts and blunders in the DEMs. First, an absolute difference threshold of 100 m was applied, which was followed by a threshold of ± 3 times the standard deviation of elevation differences over stable, off-glacier terrain (Gardelle et al., 2013; Ragetti et al., 2016). The glacier was then divided into boxes of ~600-m horizontal distance along its central flow line. The length of boxes was modified slightly near glacier confluences to assist the flux divergence calculations (see section 3.3). Elevation change statistics were computed for each box. The horizontal distance of 600-m boxes was used to compute the flux divergence and also to mitigate the effects of alternating positive and negative elevation differences caused by the advection of local glacier surface topography.

For boxes near the debris-clean ice interface, the elevation change was only measured for the debris-covered areas. Masking of elevation change data was achieved following the classification of ice using band-ratio techniques and a Landsat ETM+ scene from 2003 (Kääb et al., 2012). We assume no substantial change in debris cover extent between 2003 and 2009/2010. Furthermore, the elevation change associated with ice cliffs and supraglacial ponds on the debris-covered glaciers in each box was both excluded and included in order to assess the mixed pixel effect. The areal extent of ice cliffs and supraglacial ponds was estimated using delineations from Watson et al. (2017) from 5 June 2010, 7 June 2015, and 13 May 2015 for Ngozumpa, Khumbu, and Imja-Lhotse Shar Glaciers, respectively. The use of images around the monsoon season was assumed to be more representative of the areal extent of ice cliffs and supraglacial ponds, since pond coverage peaks at the onset of the monsoon and decreases in the winter (Miles et al., 2017).

The approach of Gardelle et al. (2013) and Ragetti et al. (2016) was used to estimate the uncertainty associated with the elevation change data for each box. The standard error ($E_{\Delta h}$) of elevation differences over stable terrain was calculated as

$$E_{\Delta h} = \frac{\sigma_{\text{stable}}}{\sqrt{N}} \quad (1)$$

where σ_{stable} is the standard deviation of elevation change over stable, off-glacier terrain, and N is the effective number of observations (Bolch et al., 2011). N is calculated through

$$N = \frac{N_{\text{tot}} \cdot \text{PS}}{2d} \quad (2)$$

where N_{tot} is the total number of DEM difference data points, PS is the pixel size, and d is the distance of spatial autocorrelation, which was assumed to be equal to 20 pixels (200 m) based on Bolch et al. (2011). The mean $E_{\Delta h}$ of all the boxes associated with each set of DEMs ranged from ± 0.47 to 0.72 m.

3.2. Horizontal Surface Velocity

Glacier surface velocities on Ngozumpa, Khumbu, and Imja-Lhotse Shar Glaciers were computed for all potential pairs of available high-resolution DEMs (GeoEye-1, WorldView-1, WorldView-2; DigitalGlobe, Inc.) from 2010 to 2016. Velocity grids were derived using the vmap tool (<https://github.com/dshean/vmap>), which uses the NASA Ames Stereo Pipeline correlator (Shean et al., 2016). Rather than using input image

data, which have variable illumination and snow cover, the correlation was run on multidirectional shaded-relief maps derived from coregistered 4-m resolution DEMs. The identical synthetic illumination and abundant texture at high-resolution provided improved correlation success. We used a 35-pixel correlation kernel size, parabolic subpixel disparity map refinement, and a filter to remove isolated disparity map clusters with area less than 1,024 pixels. Filtered disparity maps were smoothed using a 9×9 Gaussian kernel to remove residual artifacts. Velocity magnitudes in meters per year were computed based on input resolution and time interval. Since we used coregistered DEMs as inputs, no additional offset correction over static surfaces was required after correlation.

Initially, we used surface velocities associated with the specific pair of DEMs to estimate flux divergence. However, too many gaps were present in the surface velocity due to a loss of coherence, which caused issues for the flux divergence calculations (section 3.3). Therefore, we used the per-pixel median velocity from all pairs to estimate the surface velocity for each glacier. These surface velocities were devoid of gaps over the debris-covered portion of the glacier. Velocities over stable, off-glacier terrain were used to estimate the uncertainty associated with the glacier surface velocity as well as the minimum velocity that was deemed to be reliable.

3.3. Flux Divergence and Vertical Velocity

Surface velocities and ice thickness estimates (Huss & Farinotti, 2012, updated to RGI 6.0; Figure S1 in the supporting information), were used to calculate the flux divergence for each 600-m box (<https://github.com/drounce/Rounce2018JGR>). According to Cogley et al. (2011), negative flux divergence means that the box is gaining mass and is called the emergence velocity, while positive flux divergence means that the box is losing mass and is called the submergence velocity. To estimate the flux divergence, the ice flux for each 30-m pixel was computed according to

$$\vec{q} = h\gamma\vec{u}_{sfc} \quad (3)$$

where h is the ice thickness (m), γ is the ratio of the mean velocity of the ice to the surface velocity (assumed to be 0.8 for negligible basal sliding (Nuimura et al., 2011; Vincent et al., 2016)), and \vec{u}_{sfc} is the surface velocity vector (m/a). The flux divergence was computed for each pixel, and then total flux divergence was calculated within each 600-m box (Nuimura et al., 2011; Vincent et al., 2016).

The flux divergences are subject to uncertainties associated with the surface velocities, ice thickness estimates, and γ . Monte Carlo simulations were used to quantify how these uncertainties affected the flux divergences. To estimate velocity uncertainty, we considered statistics for the entire “stack” of ~100–400 velocity products available at each glacier. The surface velocity was assumed to be normally distributed around the median velocity of each pixel and have a standard deviation according to the normalized median absolute deviation (NMAD) associated with the stable, off-glacier terrain. For a normal distribution, the NMAD is equivalent to the standard deviation (Dehecq et al., 2015; Höhle & Höhle, 2009). The minimum detectable velocity, that is, the velocity below which the glacier was considered to be stagnant, was assumed to be normally distributed using the median and NMAD associated with the stable, off-glacier terrain. Additionally, clusters of higher velocities on the glacier tongues, which were an artifact of the backwasting associated with bare ice cliffs and the expansion/contraction of supraglacial ponds (see section 4.1), were manually masked prior to the flux divergence calculations and replaced with a velocity of zero.

The bias associated with the Huss and Farinotti (2012) ice thickness estimates is -21% (interquartile range of $\pm 39\%$) based on a comparison with in situ ice thickness measurements from a sample of glaciers located across the globe but outside of the Himalayan region (Farinotti et al., 2017). Initially, the bias and interquartile range was used to assess the uncertainty; however, adjusting the ice thickness for a 60% underestimation (the lower end of the interquartile range) produced ice thicknesses exceeding 1,000 m, which were considered unrealistic for the region (Gades et al., 2000; Somos-Valenzuela et al., 2014). Therefore, the uncertainty associated with the ice thicknesses assumed a uniform distribution between 0% and -21% . This range enabled the ice thickness to be corrected for potential underestimations of up to 21% but avoided producing unrealistic ice thicknesses. For each 600-m box on each glacier, 1,000 Monte Carlo simulations were run to generate a probability density function of flux divergence.

3.4. Subdebris Melt

Debris-covered glacier melt was estimated using a 1-D steady state debris-covered glacier energy balance model (Rounce et al., 2015):

$$R_n + H + LE + P + Q_c = 0 \quad (4)$$

where R_n is the net radiation flux, H is the sensible heat flux, LE is the latent heat flux, P is the heat flux supplied by rain, and Q_c is the ground heat flux (all in W/m). Each of these terms is described in detail by Rounce et al. (2015). For the ground heat flux, the debris was broken down into 10 layers to model the nonlinear temperature profiles at each time step using the Crank-Nicholson and Newton-Raphson method (Reid & Brock, 2010). The latent heat flux was estimated using the LE_{Rain} model from Rounce et al. (2015) due to the availability of precipitation data. This LE model assumes that the surface is saturated when it is raining; otherwise, LE is assumed to be zero. Additionally, the effect of topography on the incoming shortwave radiation was accounted for in this study using the 10-m DEM from 2012 for Ngozumpa Glacier and 2015 for Khumbu and Imja-Lhotse Shar Glaciers, which was then averaged to estimate the incoming shortwave radiation over each 600-m box for each time step. The effect of shading from surrounding terrain was not included. The density of ice was assumed to be 900 kg/m. A period of 5 days was used to spin-up the model.

3.5. Meteorological Data

Meteorological data from Pyramid Station (27.959°N, 86.813°E, 5035 m a.s.l., managed by EV-K²-CNR), which is located off-glacier next to Khumbu Glacier, were used for the debris-covered glacier energy balance model. The data provided by Pyramid Station were hourly air temperature, relative humidity, wind speed, precipitation, incoming shortwave radiation, and incoming longwave radiation from 2009 to 2014 between 15 May and 15 October each year (Salerno et al., 2015). A standard temperature lapse rate of 6.5 °C/km was applied to spatially extrapolate the air temperature across the glacier, which is well within the range of lapse rates observed in the Nepal Himalaya, albeit slightly higher than the average (Fujita & Sakai, 2000; Immerzeel et al., 2014). All other meteorological data were assumed to be constant over the glacier. The time period of 15 May to 15 October was used to estimate the amount of subdebris melt for each summer monsoon season. Outside of this time period, melt was assumed to be zero, which agrees well with temperature sensors in the debris that indicate the debris is frozen otherwise (Nicholson & Benn, 2012; Rounce et al., 2015). Additionally, the climatic mass balance from 15 October to 15 May is assumed to be zero; that is, any seasonal snow that may have accumulated during this period of time is assumed to have melted by 15 May. Snow depth data from Pyramid Station confirm that this is a reasonable assumption (Figure S2). However, since the model does not account for snow accumulation/melt, problems may arise with DEMs that are acquired when there is snow on the ground, which was the case for the 2014 DEM of Ngozumpa Glacier. The impact of this assumption on the elevation change and model validation is discussed in detail in section 5.4.

A variety of techniques were used to fill in gaps in the meteorological data. Short temporal gaps (<4 hr) were linearly interpolated. Data gaps in precipitation were replaced using daily reconstructed data from Salerno et al. (2015), where precipitation was downsampled to hourly estimates by distributing the precipitation over times with the highest relative humidity (typically 100%). Data gaps in wind speed data were primarily due to speeds being below the detectable limit or the instrument being offline. For long data gaps (>1 day), the instrument was assumed to be offline, so wind speed data from an automatic weather station at Kala Patthar (27.983 °N, 86.816 °E, 5,545 m a.s.l.) was used in its place. For shorter gaps (<1 day) the wind speed was assumed to be below the detectable limit and a value of 0 m/s was used. Incoming longwave radiation data were unavailable after 2012, so 6-hr National Centers for Environmental Prediction/National Center for Atmospheric Research reanalysis data (Kalnay et al., 1996) with the minor modification of reducing the National Centers for Environmental Prediction/National Center for Atmospheric Research estimate by 29 W/m (Rounce et al., 2015) were linearly interpolated to provide hourly data. Due to a lack of reliable snow measurements, the model assumes a snow-free surface. This snow-free assumption affects 6% of the data between 2009 and 2014; that is, the meteorological data suggested that 6% of the time there was snow on the ground, but we assumed a snow-free surface. These snow measurements primarily occurred during transition seasons when melt rates are relatively small, so the total impact on the model is assumed to be negligible.

Table 2
Summary of the Number of Days in Each Month That Are Missing Meteorological Data Over the Span of the Study Period (2009–2014)

Year	Month						Total
	May	Jun	Jul	Aug	Sept	Oct	
2009	2	—	—	—	—	—	2
2010	2	14	28	—	3	3	50
2011	2	14	1	—	—	—	17
2012	10	15	—	—	—	—	25
2013	14	4	18	—	—	—	36
2014	17	—	1	9	6	3	36

Note. The study only includes dates between 15 May and 15 October each year.

For other meteorological data that had data gaps greater than 4 hr that could not be filled using the methods described above, the entire day was discarded. This affected 18% of the data and as much as 32% for a given year (Table 2). For these missing days, the daily melt was assumed to be equal to the average daily melt rate for that month. If data for the entire month was unavailable (e.g., May 2014), then the average daily melt was assumed to be equal to the average daily melt rate for that month over the entire study period.

3.6. Debris Thickness Estimates

The continuity equation shows the relationship between the rate of change of glacier thickness (\dot{h}), climatic-basal mass balance (\dot{b}), and flux divergence ($\nabla \cdot \vec{q}$) (Cogley et al., 2011):

$$\dot{h} = \dot{b} - \nabla \cdot \vec{q} \quad (5)$$

This study assumes that \dot{h} is equal to the rate of elevation change. \dot{b} is assumed to equal the surface mass balance rate as the basal, and internal mass balance components are assumed to be negligible. Surface accumulation due to surface meltwater refreezing is also assumed to be negligible. Since the climatic mass balance is assumed to be zero between 15 October and 15 May, and the debris is considered to be snow free (see section 3.5), the continuity equation is used to estimate the observed subdebris melt rate.

We iteratively solved for the debris thickness by inverting the Østrem curve (Østrem, 1959) such that the modeled subdebris melt rate agreed with the observed subdebris melt rate based on the elevation change and flux divergence for each 600-m box (<https://github.com/drounce/Rounce2018JGR>). The debris thickness was assumed to be constant over the course of the study period; that is, the model does not account for the redistribution of debris. This method of inverting a debris-covered glacier energy balance model to estimate debris thickness is similar to Ragetti et al. (2015); however, this study includes the ice flux divergence, accounts for topography, and quantifies uncertainty. Hereon, the method will be referred to as the MC-Østrem inversion method. The debris thickness was iteratively adjusted to the nearest 0.01 m until the modeled subdebris melt rate agreed with the measured subdebris melt rate (Figure 2). A minimum debris thickness of 0.02 m was used as this is approximately the critical thickness below which the thin layer of debris enhances melting compared to clean ice (Kayastha et al., 2000; Mattson et al., 1993; Østrem, 1959). If the measured subdebris melt rate exceeded the modeled melt rate associated with a debris thickness of 0.02 m, the debris thickness was assumed to be 0.02 m. A maximum debris thickness of 5 m was also used as this is approximately the maximum debris thickness in the region (Nicholson, 2004). If the measured subdebris melt rate was less than the modeled subdebris melt rate associated with a debris thickness of 5 m, the debris thickness was assumed to be 5 m.

Monte Carlo simulations were used to account for the uncertainty associated with the debris properties (albedo, surface roughness, and thermal conductivity), flux divergence, and elevation change (Figure 2). The albedo was assumed to have a uniform distribution between 0.1 and 0.4 (Inoue & Yoshida, 1980; Kayastha et al., 2000; LeJeune et al., 2013; Nicholson & Benn, 2012), the surface roughness was assumed to

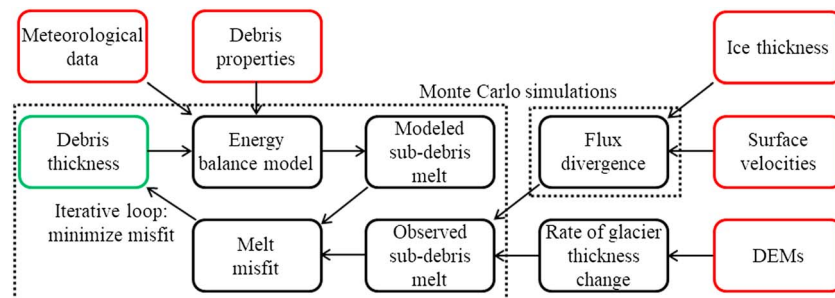


Figure 2. Schematic of the MC-Østrem inversion method showing the input (red), method components (black), and debris thickness output (green) along with the portions of the method that include Monte Carlo simulations (dotted boxes).

have a uniform distribution between 0.0035 and 0.0600 m (Brock et al., 2010; Inoue & Yoshida, 1980; Quincey et al., 2017; Takeuchi et al., 2000), and the thermal conductivity was assumed to have a uniform distribution between 0.47 and 1.62 $\text{W} \cdot \text{m}^{-1} \cdot \text{K}^{-1}$ (Conway & Rasmussen, 2000; Nicholson & Benn, 2012; Rounce et al., 2015; Rounce & McKinney, 2014). The uncertainties associated with the flux divergence were accounted for by randomly sampling the probability density function (see section 3.3). The uncertainty associated with the measured elevation change was accounted for assuming a normal distribution (see section 3.1). For each 600-m box, 1,000 simulations were used to generate a probability density function of debris thickness from which the median and other statistics were computed.

3.7. Method Calibration and Validation

The time series of DEMs for Ngozumpa Glacier (Table 1) was used to calibrate and validate the debris thickness estimates. Specifically, the debris thickness was calibrated using the MC-Østrem inversion method with the observed subdebris melt rates, that is, the combination of the measured elevation change (section 3.1) and modeled flux divergence (section 3.3), from 2010 to 2012. This generated a probability density function of debris thickness for each 600-m box. The method was then validated by comparing the observed subdebris melt rates from 2012 to 2014 with the modeled subdebris melt rates based on the calibrated debris thickness. The modeled subdebris melt rates from 2012 to 2014 were estimated using 1,000 Monte Carlo simulations, which accounted for the uncertainty of the calibrated debris thicknesses using the probability density functions for each box. The uncertainty of the other debris properties (albedo, surface roughness, and thermal conductivity) and the flux divergence were also included in these Monte Carlo simulations (section 3.6).

The calibrated debris thickness estimates from 2010 to 2012 were also compared to two sets of existing field measurements. The first set was made by surveying debris exposed above ice cliffs (Nicholson & Benn, 2012). Within this set, there were two groups of measurements located 1 ($n = 94$) and 7 km ($n = 124$) from the glacier terminus. The second set was made using ground-penetrating radar (GPR; Nicholson & Mertes, 2017). The second set was also broken down into two groups located 1 ($n = 13,984$) and 2.3 km ($n = 130,925$) from the glacier terminus. Measurements of debris thickness made by surveying debris exposures above ice cliffs and GPR constitute the best available ground-truth data as neither is biased toward thinner debris, which is typically the case for pit measurements.

Observed subdebris melt rates based on elevation change and flux divergence estimates were also used to estimate the debris thickness for Khumbu and Imja-Lhotse Shar Glaciers. These debris thickness estimates were compared to existing measurements on Khumbu Glacier (Nakawo et al., 1986) and Imja-Lhotse Shar Glacier (Rounce & McKinney, 2014).

4. Results

4.1. Horizontal Surface Velocity

The surface velocities on Ngozumpa, Khumbu, and Imja-Lhotse Shar Glaciers show that the maximum velocity occurs near the transition from clean ice to debris cover and the velocity decreases toward the terminus of the glacier (Figure 3). On Ngozumpa Glacier (Figure 3a), the velocity peaks around 140 m/a at the transition from clean ice to debris cover and becomes relatively stagnant (<5 m/a) around 6.3 km from the glacier terminus. On Khumbu Glacier (Figure 3b), the velocity peaks beneath the Khumbu icefall around 100 m/a and decreases downglacier until it begins to stagnate (<5 m/a) around 3.7 km from the terminus. The true location of the peak velocity for Khumbu Glacier is difficult to identify as there are gaps in surface velocity over and beneath the Khumbu icefall. The velocity on Imja-Lhotse Shar Glacier (Figure 3c) similarly peaks around 100 m/a near the transition from clean ice to debris cover on Lhotse Shar Glacier. Lhotse Shar Glacier appears to be fairly active and its velocity gradually decreases downglacier, while Imja Glacier appears to stagnate (<5 m/a) around 0.75–1.5 km behind Imja Tsho.

On the tongues of Ngozumpa and Khumbu Glaciers there are clusters of higher velocities (5–15 m/a), which coincided with the location of ice cliffs and supraglacial ponds (Figure 3). The error associated with the surface velocity was assessed over stable, off-glacier terrain. The median (\pm NMAD) velocity magnitude over stable terrain was 4.4 (± 2.1), 4.1 (± 2.6), and 5.5 (± 3.7) m/a for Ngozumpa, Khumbu, and Imja-Lhotse Shar

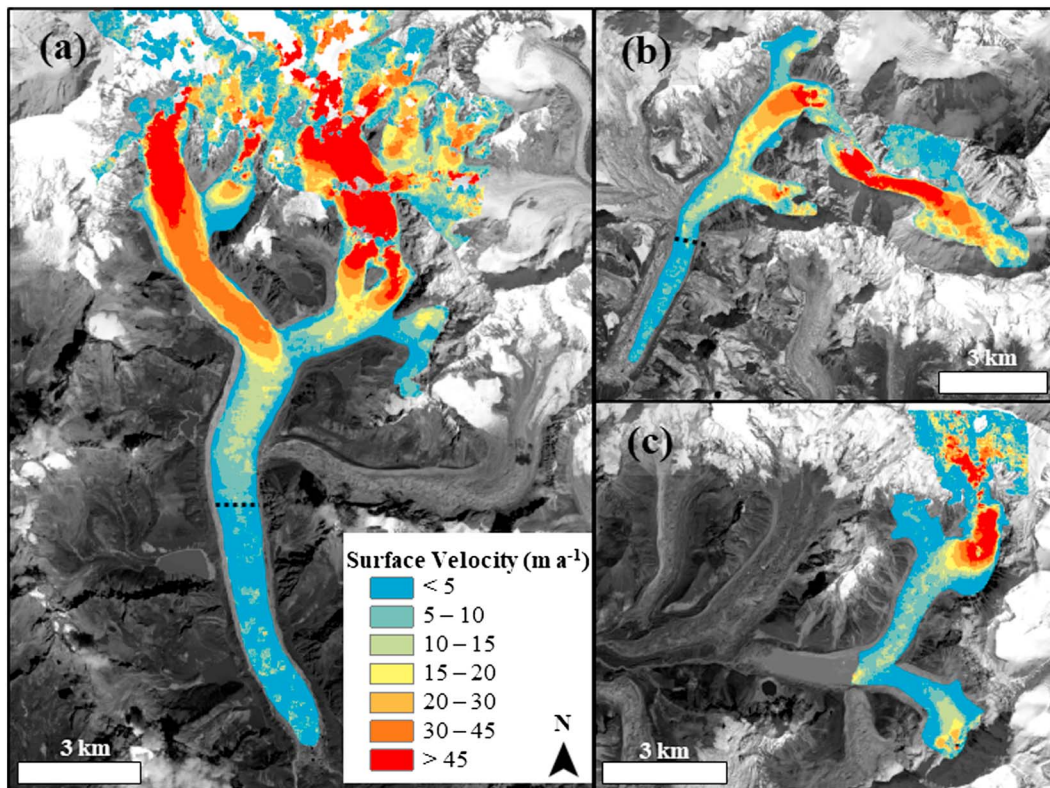


Figure 3. Median surface velocities over (a) Ngozumpa, (b) Khumbu, and (c) Imja-Lhotse Shar Glaciers based on all potential pairs of available high-resolution digital elevation models (DEMs) from 2010 to 2016. Dashed lines indicate where Ngozumpa and Khumbu Glaciers appear to stagnate. The 2014 lake extent of Imja Tsho has been removed. Background image is Landsat 8 from 30 September 2015.

Glaciers, respectively. These statistics were used to estimate the minimum velocity in the flux divergence calculations. The uncertainty associated with the velocity at each pixel was estimated using the NMAD.

4.2. Flux Divergence and Vertical Velocity

Horizontal surface velocity and ice thickness estimates were used to estimate the flux divergence for each 600-m box on Ngozumpa, Khumbu, and Imja-Lhotse Shar Glaciers (Figure 4). On the debris-covered portion of the glacier, the flux divergence was negative, indicating emergence, for all the boxes with the exception of

the box 11.2 km from the terminus of Ngozumpa Glacier. The positive flux divergence for this one box was caused by an apparent bottleneck in the surface velocity (Figure 3a), which is considered to be an artifact associated with the surface velocity estimate, since it is highly unlikely for this area of the ablation zone to have a submergence velocity. The negative flux divergence associated with all the other boxes, hereon referred to as emergence velocity and described as positive values of emergence, ranged from zero on the stagnant glacier tongues to a maximum of 4.2 (± 0.3), 4.0 (± 0.3), and 4.6 (± 0.3) m/a for Ngozumpa, Khumbu, and Imja-Lhotse Shar glaciers, respectively (parentheses indicate NMAD). In general, the emergence velocity peaked below the transition from clean ice to debris cover and then steadily decreased downglacier until the glacier became stagnant. For Ngozumpa and Khumbu Glaciers, the maximum emergence velocity was located around 1 km below the transition from clean ice to debris cover. The emergence velocities beneath the Khumbu icefall (6.7–8.4 km from the terminus) ranged from 0.8 to 4.3 m/a, which

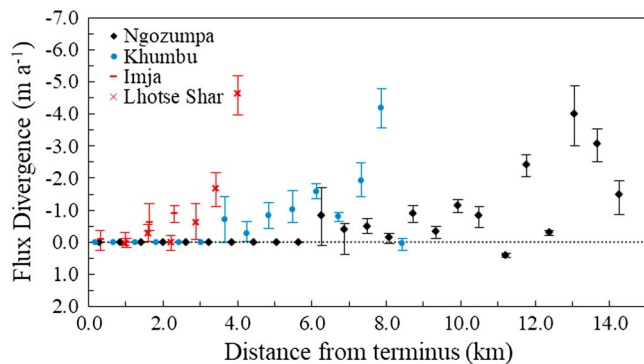


Figure 4. Flux divergence for each 600-m box on the main branch of Ngozumpa, Khumbu, and Imja-Lhotse Shar Glaciers showing the median and normalized median absolute deviation. Boxes over stagnant portions of the glacier have a flux divergence of zero. Note that the y axis is inverted such that emergence velocities are above the dashed line.

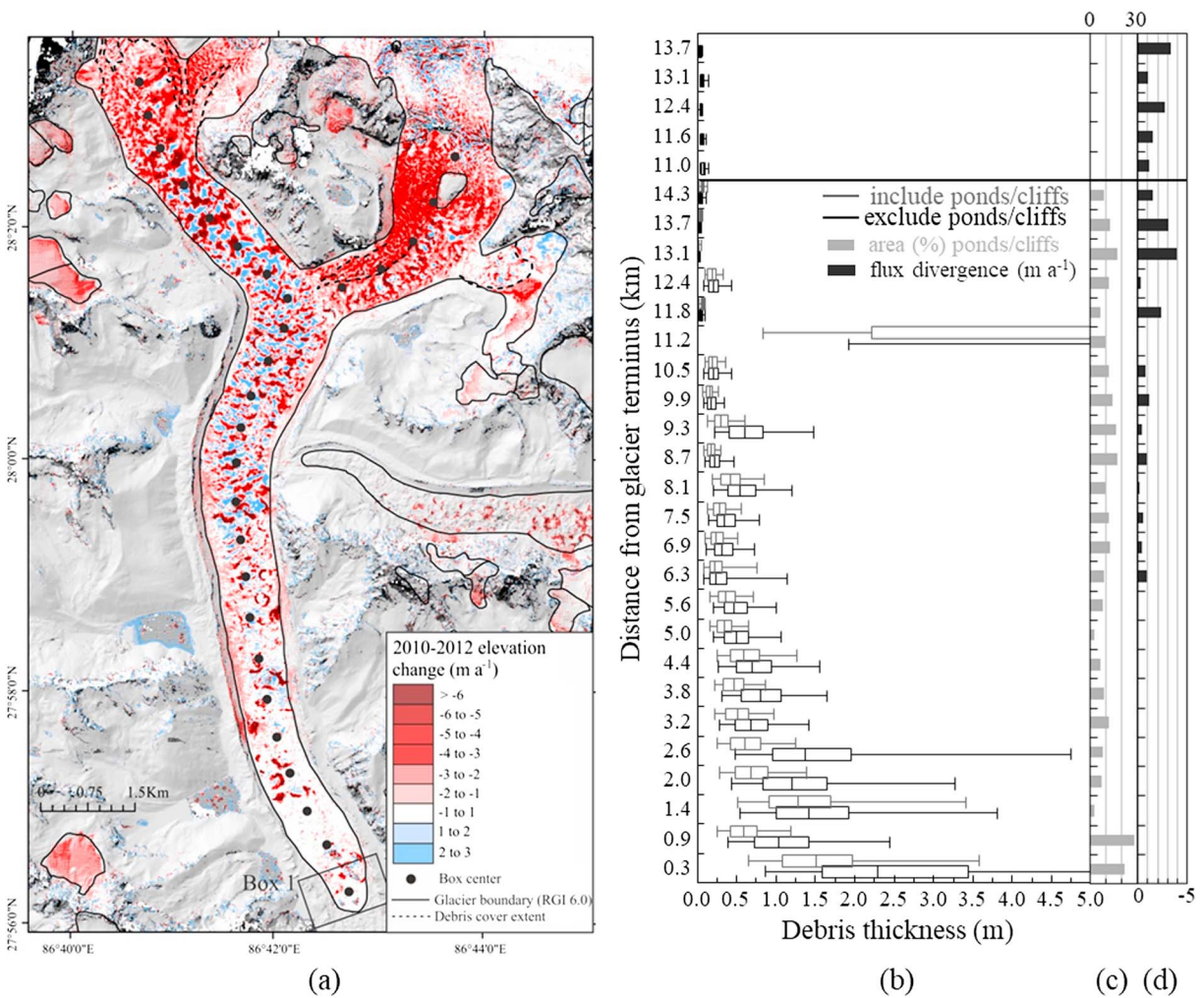


Figure 5. (a) Elevation change on Ngozumpa Glacier from 2010 to 2012, (b) a box-and-whisker plot showing the distribution of debris thickness estimates within each box as a function of distance from the glacier terminus for the MC-Østrem inversion method both including (gray) and excluding (black) supraglacial ponds and ice cliffs, and box plots showing (c) the percent of the total area in each box that is ponds and cliffs (Watson et al., 2017) and (d) the median flux divergence. The whiskers denote the 95% confidence bounds. Black points along the glacier centerline indicate the center of the 600-m boxes.

are similar to the emergence velocity of 5.1 m/a estimated by Nuimura et al. (2011) for a similar area.

4.3. Ngozumpa Glacier

4.3.1. Debris Thickness Calibration

The inverse ablation gradient typical of debris-covered glaciers, that is, an increase in surface lowering upglacier where the debris cover is thinner, is clearly evident on Ngozumpa Glacier (Figure 5a). Local variability in surface lowering can be seen in boxes over the high-velocity regions of the glacier (Figure 3), where the advection of local glacier surface topography caused alternating positive and negative elevation differences. Local maxima in surface lowering are evident over much of the stagnant part of the main glacier tongue where ice cliffs and supraglacial ponds were present.

Debris thicknesses required to model the observed subdebris melt, that is, the combination of elevation change and flux divergence, vary by an order of magnitude over the ablation zone and show a general trend of the debris thickness decreasing upglacier (Figure 5b). The one exception is the box located 11.2 km from the terminus, which is considered to be an artifact of the flux divergence calculations (see section 4.2). The maximum box-wide median debris thickness of 2.29 m was located at the terminus, and the median debris thickness gradually decreased to less than 0.20 m beyond 9.9 km from the terminus (Figure 5b). The confidence interval associated with the thicker debris near the terminus was much wider because small

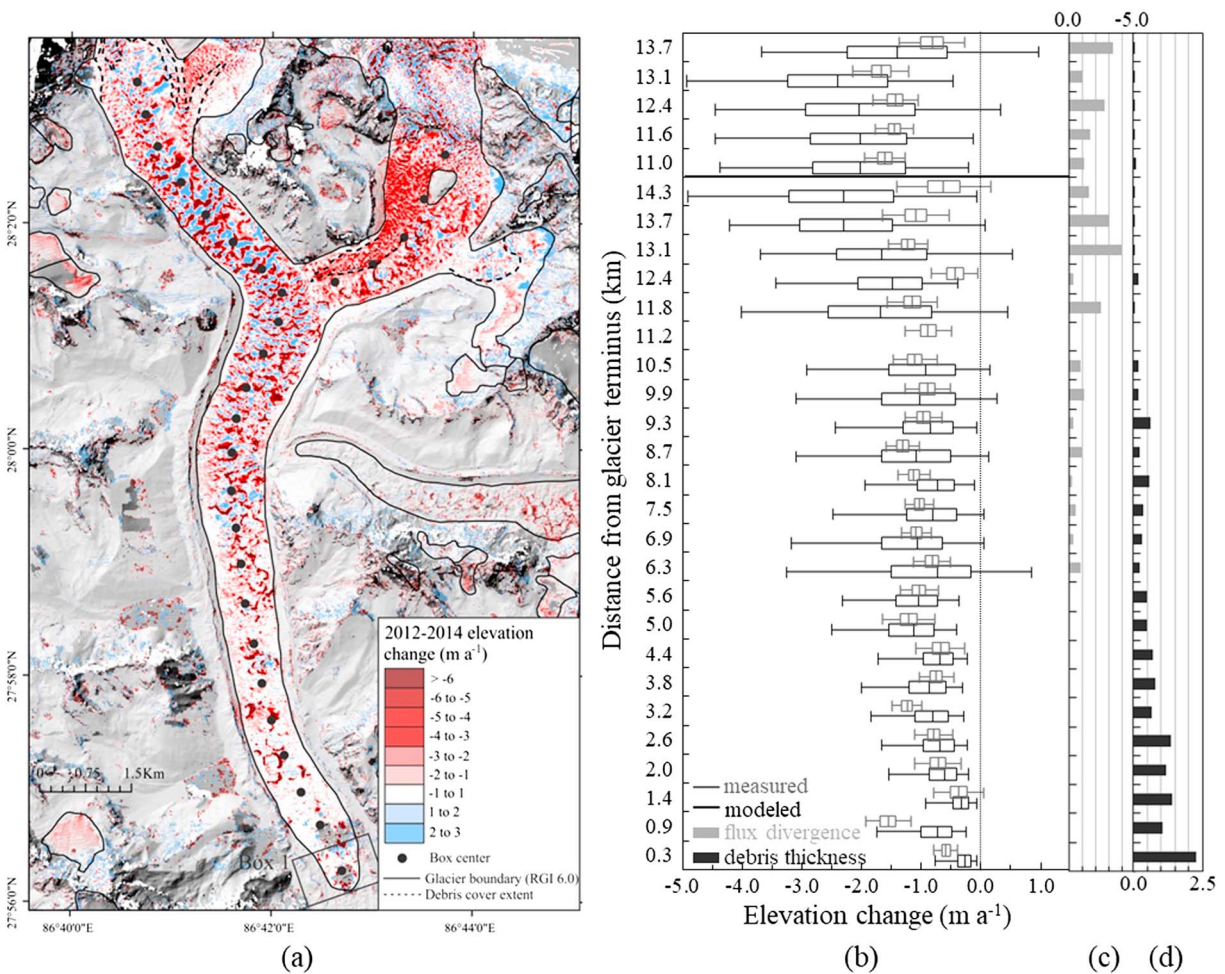


Figure 6. (a) Elevation change on Ngozumpa Glacier from 2012 to 2014, (b) a box-and-whisker plot showing the distribution of measured surface lowering (gray) and modeled surface lowering (black) for each box, and box plots of the (c) median flux divergence (m/a ; light gray) and (d) median debris thickness (m ; dark gray). The whiskers denote the 95% confidence bounds. Black points along the glacier centerline indicate the center of the 600-m boxes.

changes in thick debris (>0.5 m) do not alter the modeled subdebris melt rate as much as the equivalent changes for thinner debris (<0.5 m). Therefore, when the Monte Carlo simulations altered the observed subdebris melt rate based on the uncertainty associated with the elevation change and flux divergence, the adjustments in debris thickness required for the modeled subdebris melt rate to agree are larger in boxes where the debris is thick.

A comparison of debris thickness estimates derived from including and excluding ice cliffs and supraglacial ponds illustrates the mixed pixel effect or “mixed box” effect as it is referred to in this study (Figure 5b). The mixed box effect is a function of the debris thickness and the prevalence of ponds and cliffs, that is, at the terminus of the glacier the median debris thickness is 0.79 m thinner due to the prevalence of cliffs and ponds (22% of glacier surface area in the box) and the thick debris (median of 2.29 m). However, further upglacier (>6 km from the terminus), ponds, and cliffs are still prevalent, yet the mixed pixel effect only slightly reduces the debris thickness because the debris is much thinner (<0.5 m). The relationship between debris thickness, ice cliff, and supraglacial pond density, and surface lowering was also observed by Thompson et al. (2016) and Watson et al. (2017).

4.3.2. Debris Thickness Validation

The calibrated debris thicknesses and emergence velocities were used to estimate the elevation change from 2012 to 2014 and were compared to the measured elevation change of each box in order to assess the performance of the MC-Østrem inversion method. The calibrated debris thicknesses derived from including the surface lowering of ice cliffs and supraglacial ponds was used in order to reduce the errors associated

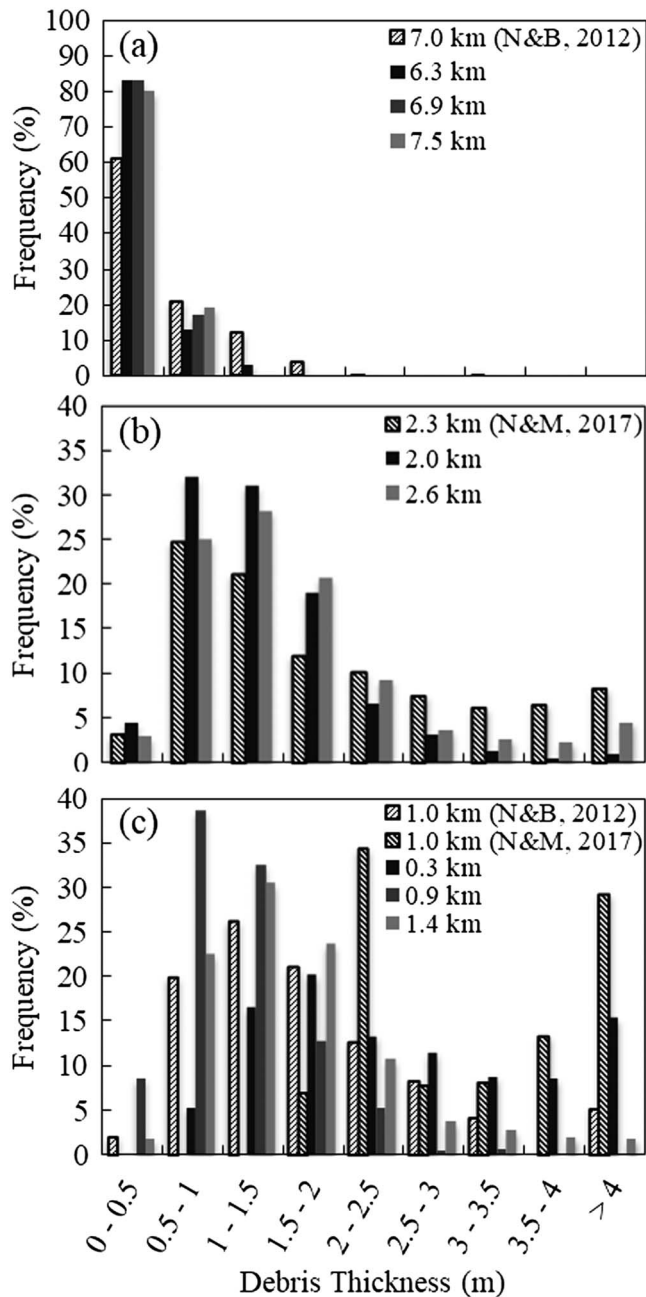


Figure 7. Comparison of the calibrated MC-Østrem debris thickness estimates derived by excluding supraglacial ponds and ice cliffs on Ngozumpa Glacier with in situ debris thickness measurements made by surveying exposed ice cliffs (Nicholson & Benn, 2012, abbreviated as “N&B, 2012”) and ground-penetrating radar (Nicholson & Mertes, 2017, abbreviated as “N&M, 2017”) (a) 7 km, (b) 2.3 km, and (c) 1 km from the terminus.

ness yielded significantly different distributions as well. The range of the debris thickness estimates also appears to capture the natural variability of the measured debris thickness, which further supports the performance of the MC-Østrem inversion method.

4.4. Khumbu Glacier

Debris thickness on Khumbu Glacier was estimated from the flux divergence and elevation change between 2009 and 2015 (Table 1). The inverse ablation gradient described for Ngozumpa Glacier was also evident on

with spatial and temporal changes in the areal extent of cliffs and ponds. Figure 6 shows the modeled surface lowering, that is, negative elevation change, increases upglacier due to the decreasing debris thickness. For 24 of the 28 boxes, the 95% confidence interval of the measured surface lowering rates was contained within the 95% confidence interval of the modeled surface lowering rates (Figure 6b). A Wilcoxon rank sum test revealed that the median modeled and measured surface lowering rates for 3 of the 28 boxes (4.4, 5.6, and 6.9 km from the terminus) are not significantly different ($\alpha = 5\%$), while the other 25 boxes rejected the null hypothesis of having equal medians.

For the lower 11 km of the glacier, that is, the area located beneath the junction of the two branches from Cho Oyu and Gyachung Kang, the median absolute difference between the median measured and modeled surface lowering rates was 0.13 m/a, while above this junction the median difference was 0.56 m/a. With the exception of the second box located 0.9 km from the terminus, the greatest difference between the median measured and modeled surface lowering rates coincided with the boxes with the largest flux divergences. These boxes also had the widest 95% confidence intervals, which were approximately three times wider than boxes on the stagnant portion of the glacier.

For all the boxes, the confidence intervals of the modeled elevation change were significantly larger than those of the measured elevation change (Figure 6b). The wider confidence intervals were a result of the MC-Østrem inversion method accounting for the uncertainty associated with the debris properties (debris thickness, albedo, surface roughness, and thermal conductivity) and flux divergence. Hence, the difference in confidence intervals highlights the importance of advancing our understanding of the debris properties and glacier dynamics in order to improve our ability to forecast glacier melt in the future.

The performance of the MC-Østrem inversion method was also assessed by comparing the debris thicknesses derived by excluding the supraglacial ponds and ice cliffs with in situ debris thickness measurements from Ngozumpa Glacier (Nicholson & Benn, 2012; Nicholson & Mertes, 2017). Both the calibrated and measured debris thicknesses show the debris thickness decreases upglacier (Figure 7). Around 7 km from the terminus (Figure 7a), the mean (\pm standard deviation)-calibrated debris thickness was 0.35 m (± 0.21 m) compared to the measured thickness of 0.59 m (± 0.50 m). Around 2.3 km from the terminus (Figure 7b), the mean-calibrated debris thickness was 1.48 m (± 0.88 m) compared to the measured thickness of 1.95 m (± 1.27 m). Around 1 km from the terminus (Figure 7c), the mean-calibrated debris thickness was 1.76 m (± 1.09 m) compared to the measured thicknesses of 1.80 m (± 1.21 m) and 3.3 m (± 1.19 m) based on surveying and GPR, respectively. These results suggest that the debris thickness estimates from the MC-Østrem inversion method agree well with in situ measurements, especially when one considers that the different methods used to measure debris thick-

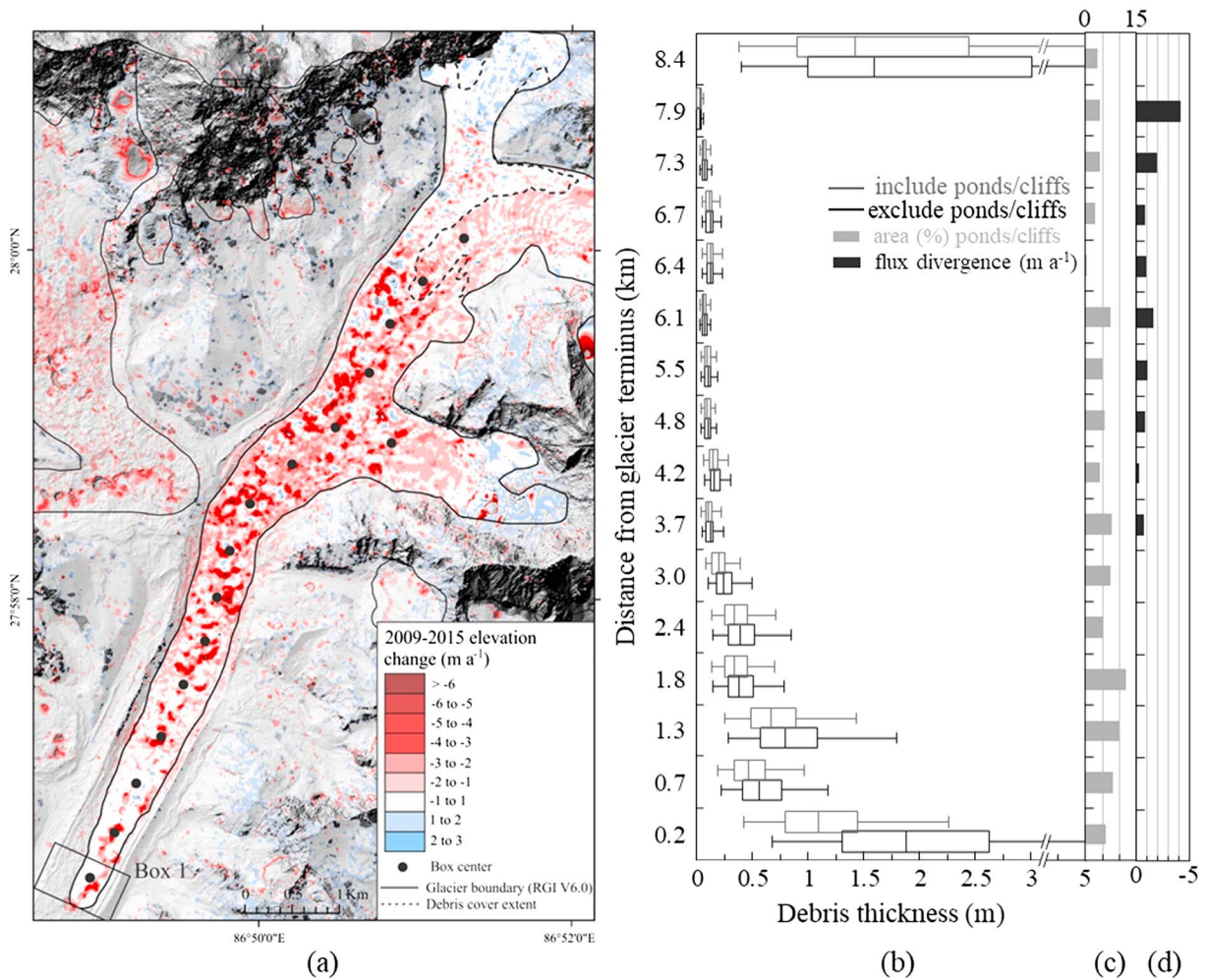


Figure 8. (a) Elevation change on Khumbu Glacier from 2009 to 2015, (b) a box-and-whisker plot showing the distribution of debris thickness estimates within each box as a function of distance from the glacier terminus for the MC-Østrem inversion method both excluding (black) and including (gray) supraglacial ponds and ice cliffs, and box plots showing (c) the percent of the total area in each box that is ponds and cliffs (Watson et al., 2017) and (d) the median flux divergence. The whiskers denote the 95% confidence bounds. Black points along the glacier centerline indicate the center of the 600-m boxes.

Khumbu Glacier (Figure 8a). Localized surface lowering was pervasive over the lowermost 3–4 km of the glacier, where ice cliffs and supraglacial ponds were present. On the western side of the glacier beneath the Khumbu icefall, the glacier has experienced relatively little mass loss likely due to the significant flux divergence in this area (Figure 8a). Bolch et al. (2011) also found that this area had very little elevation change over a much longer time period (1970–2007).

The MC-Østrem inversion debris thicknesses reflect the spatial variations in elevation change and flux divergence (Figure 5b) with a clear trend of the debris thickness decreasing upglacier. The one exception was the box located immediately below the Khumbu icefall 8.4 km from the terminus, which should be much thinner (Nakawo et al., 1986; Rounce & McKinney, 2014). The uncharacteristically thick debris in this box is considered to be an artifact of the flux divergence calculations (Figure 5d) due to a lack of surface velocities upglacier of this box and potential errors regarding the glacier thickness.

The maximum box-wide median debris thickness of 1.89 m was located at the terminus of the glacier, and the median debris thickness gradually decreased to less than 0.20 m beyond 3.4 km from the terminus (Figure 8b). Similar to Ngozumpa Glacier, the confidence interval associated with the thicker debris near the terminus was much wider than the thinner debris upglacier. These debris thickness estimates were compared to Nakawo et al. (1986), which produced a debris thickness map based on 50 measurements on the Khumbu Glacier in 1980. The maximum debris thickness of 1.89 m agrees well with their maximum of ~2 m, and both show

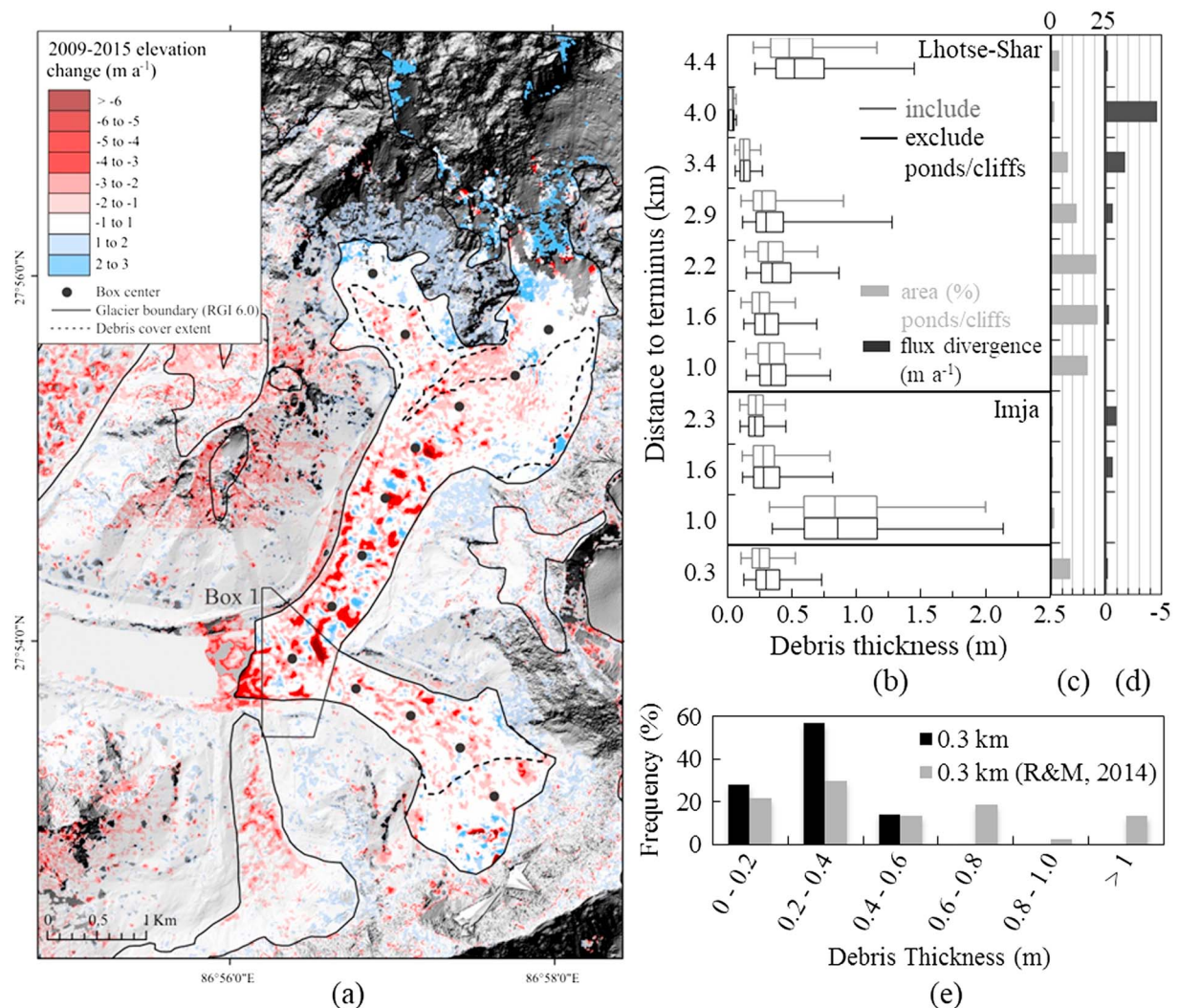


Figure 9. (a) Elevation change on Imja-Lhotse Shar Glacier from 2009 to 2015, (b) a box-and-whisker plot showing the distribution of debris thickness estimates within each box as a function of distance from the glacier terminus for the MC-Østrem inversion method both excluding (black) and including (gray) supraglacial ponds and ice cliffs, and box plots showing (c) the percent of the total area in each box that is ponds and cliffs (Watson et al., 2017), (d) the median flux divergence, and (e) a comparison of measured and estimated debris thickness. The whiskers denote the 95% confidence bounds. Black points along the glacier centerline indicate the center of the 600-m boxes.

that the debris thickness decreases exponentially upglacier to less than 0.5 m. The major difference occurs 2–6 km from the terminus, where Nakawo et al. (1986) observed thick debris (>0.5 m), while the MC-Østrem inversion method estimates the median debris thickness to range from 0.09 to 0.34 m.

The debris thicknesses derived by excluding and including supraglacial ponds and ice cliffs show that for the thick debris located within 2 km of the terminus the mixed box effect reduces the median debris thickness by 0.10–0.80 m. Further upglacier where the debris thickness is less than 0.5 m, the mixed box effect reduces the median debris thickness by less than 0.05 m.

4.5. Imja-Lhotse Shar Glacier

Debris thickness on Imja-Lhotse Shar Glacier was also estimated from flux divergences and elevation changes from 2009 to 2015 (Table 1). The elevation change showed that the glacier has experienced significant mass loss at its glacier terminus due to the expansion of Imja Tsho (Figure 9a). Upglacier from the terminus, localized surface lowering from ice cliffs and supraglacial ponds was prevalent and Lhotse Shar Glacier appeared to have more surface lowering than Imja Glacier. Additionally, areas of alternating positive and negative elevation change were apparent on Lhotse Shar Glacier but not on Imja Glacier. These areas were likely

caused by the advection of local glacier surface topography, which is consistent with the differences in surface velocities between the two branches (Figure 3c). Similar to Khumbu Glacier, the areas near the transition from debris-covered to clean ice appeared to experience less elevation change.

The box-wide debris thickness estimates on Imja-Lhotse Shar Glacier varied from a maximum median of 0.84 m located on Lhotse Shar Glacier to a minimum of 0.20 and 0.03 m for Imja and Lhotse Shar Glaciers, respectively (Figure 9b). The debris thickness appeared to decrease upglacier; however, the trend was not as prevalent as it was on Ngozumpa and Khumbu Glaciers likely because the thicker debris that would normally be located at the terminus of the glacier has been removed by the expansion of Imja Tsho. The mixed box effect was also less prevalent on Imja-Lhotse Shar Glacier with a maximum reduction in median debris thickness of 0.05 m, which was likely due to the generally thinner debris on the glacier. The estimated median (\pm NMAD) debris thickness of the box located behind the calving front was 0.29 (\pm 0.13 m) compared to 0.54 m (\pm 0.36 m) measured by Rounce and McKinney (2014; Figure 9c).

5. Discussion

5.1. Modeled Debris Thickness

The debris thickness estimates derived using the MC-Østrem inversion method agreed well with existing measurements on Ngozumpa Glacier (Figure 7). A comparison of modeled and measured elevation change during the validation period (2012–2014) also revealed that the modeled 95% confidence interval captured the measured 95% confidence interval in 24 of the 28 boxes (Figure 6b). The combination of in situ debris thickness measurements and elevation change data to assess the method's performance is a major improvement as it leverages the spatially continuous elevation data to validate estimates over the entire glacier while ensuring that debris thickness estimates are reasonable and not an artifact of the energy balance model. This dual means of validation is particularly important when one considers that typically only a limited number of debris thickness measurements are available over a small area of the glacier and these measurements can vary by an order of magnitude (Figure 7c). To the authors' knowledge, this is the first time that debris thickness estimates have been properly validated with independent data sets over an entire glacier.

The MC-Østrem inversion method also creates a step-change in our ability to estimate debris thickness as it is able to estimate thicker debris (>0.5 m) and uses Monte Carlo simulations to quantify the uncertainties associated with the debris properties, flux divergences, and elevation changes. For example, on Ngozumpa and Khumbu Glaciers, the maximum box-wide median debris thickness was 2.29 and 1.88 m, respectively, compared to thermal approaches, which estimated the median debris thickness to be 0.27 and 0.34 m, respectively (Rounce & McKinney, 2014). Interestingly, the uncertainty associated with the debris thickness estimates is a function of the debris thickness such that thinner debris had narrower 95% confidence intervals (Figure S3). This occurs because a small change in debris thickness for thinner debris (<0.5 m) can greatly alter the subdebris melt rate, while thicker debris requires a greater change in debris thickness in order to alter the subdebris melt rate to the same extent. Figure 7 shows the range of debris thickness estimates appears to capture the natural variations in measured debris thickness, although more detailed investigations are needed to determine if this is simply a coincidence or actually a reflection of the uncertainties of the debris properties being properly accounted for.

5.2. Mixed Box Effect

Debris thickness was estimated using elevation change data that both included and excluded surface lowering associated with ice cliffs and supraglacial ponds in order to quantify the mixed box effect. For thermal approaches, the mixed pixel effect refers to pixels comprising debris, ice cliffs, and supraglacial ponds, which ultimately reduces the surface temperature of the pixel and causes the debris thickness to be underestimated. In this study, each 600-m box included debris, cliffs, and ponds. The melt associated with cliffs and ponds is greater than the melt beneath debris, so the inclusion of cliffs and ponds causes the observed surface lowering to be greater. This study found that for boxes where cliffs and ponds comprised at least 5% of the area, there was a clear relationship between debris thickness and the mixed box effect (Figures 5b, 8b, and 9b). Specifically, as the debris thickness increased, the impact of the mixed box effect increased. This relationship was expected since the difference in melt rates associated with cliffs and ponds versus debris thickness increases as the debris thickness increases. For thicker debris (>0.5 m), the reduction in median debris thickness due to the mixed box effect ranged from 0.1 to 0.8 m compared to thinner debris

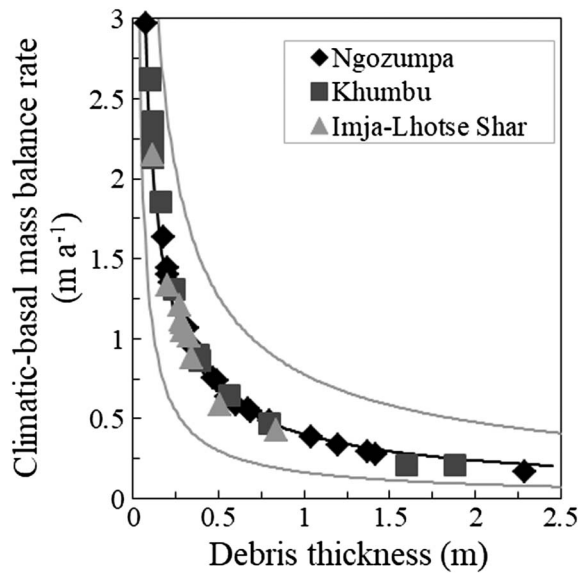


Figure 10. Relationship between the modeled climatic-basal mass balance rate and debris thickness for Ngozumpa, Khumbu, and Imja-Lhotse Shar Glaciers.

(<0.5 m), which was reduced by less than 0.1 m. This suggests that the mixed box effect has less of an impact on thinner debris. However, it is important to consider that any reductions in debris thickness for thin debris could significantly increase the subdebris melt rates, since thin debris is located on the steepest part of the Østrem curve (Figure 10).

The decision to include or exclude cliffs and ponds from the debris thickness estimates should be made based on the intended application of the estimates. In this study, the debris thickness estimates excluding cliffs and ponds were used to compare with in situ measurements in order to reduce the errors associated with the mixed box effect. On the other hand, the estimates that included cliffs and ponds were used for the validation in order to reduce the errors associated with the temporal and spatial changes in cliffs and ponds. Recent studies have found that the areal extent of cliffs and ponds can have significant temporal and spatial variations depending on the year and/or the season (Miles et al., 2017; Watson et al., 2016, 2017). Miles et al. (2017) found that the percentage of pond coverage peaks at the onset of the monsoon and then gradually decreases as they drain during the monsoon and freeze during the winter. Hence, if a winter image was used to determine the areal extent of cliffs and ponds that would be masked from the debris thickness estimates, then their actual areal extent may be underestimated. Since most of the images used

in this study were from the winter (Table 1), the areal extents associated with cliffs and ponds for each glacier from Watson et al. (2017) were used to mask the cliffs and ponds. Additionally, the advection of active portions of the glaciers can substantially alter the spatial distribution of ice cliffs, so caution should be used when masking cliffs and ponds over active areas.

The spatial and temporal changes associated with cliffs and ponds suggest that there is a balance between using elevation changes associated with a longer period of time and the impact of the mixed box effect. Specifically, a longer time series would be better suited to capture long-term trends in mass balance and likely reduce errors associated with poor meteorological data (e.g., data gaps). However, a longer time series will also make it more difficult to mask out cliffs and ponds, thereby increasing the chances of the mixed box effect impacting the debris thickness estimates.

5.3. Debris Properties and Uncertainties

Monte Carlo simulations were used to incorporate uncertainties associated with the albedo, surface roughness, thermal conductivity, flux divergence, and elevation change into the debris thickness estimates. Specifically, the R^2 value (coefficient of determination) associated with each source of uncertainty and the debris thickness for each box on each glacier was computed ($n = 1,000$). The p values associated with the R^2 values were all less than 0.01 indicating that the linear regressions were significant at this level. Table 3 shows the mean values of R^2 associated with all the boxes for each glacier. The trends are roughly the same for each glacier with the thermal conductivity having the highest R^2 value of 0.39–0.55 indicating that the uncertainty associated with the thermal conductivity contributes the most to the uncertainty associated with the debris thickness estimates. For Ngozumpa and Khumbu Glaciers, the errors associated with the elevation change had the second highest R^2 values (0.14–0.19, respectively), while for Imja-Lhotse Shar Glacier, the

Table 3
 R^2 Values Showing the Relationship Between Debris Thickness and Sources of Uncertainty (Debris Properties, Elevation Change, and Flux Divergence)

Glacier	R^2 values, mean (standard deviation)				
	Albedo	Surface roughness	Thermal conductivity	Elevation change	Flux divergence
Ngozumpa	0.11 (0.08)	0.06 (0.03)	0.47 (0.17)	0.19 (0.15)	0.11 (0.11)
Khumbu	0.10 (0.06)	0.10 (0.03)	0.55 (0.14)	0.14 (0.15)	0.09 (0.08)
Imja-Lhotse Shar	0.07 (0.06)	0.12 (0.04)	0.39 (0.12)	0.11 (0.07)	0.18 (0.10)

Note. The p values were all less than 0.01 indicating that they are significant at this level.

error associated with the flux divergence had the second highest R^2 value. The R^2 values associated with the other parameters were similar indicating that the uncertainty associated with each parameter influenced the debris thickness estimates to a similar extent.

The distributions used in the Monte Carlo simulations were based on existing in situ measurements of surface properties (section 3.4), the error associated with the elevation change (section 3.1), and the uncertainty of the flux divergence (section 3.3). Therefore, the R^2 values reflect the sensitivity of the debris thickness estimates to each parameter, which can provide guidance for future work. Specifically, the most important parameter for debris thickness estimates is thermal conductivity, which displays significant variations ($0.47\text{--}1.62\text{ W} \cdot \text{m}^{-1} \cdot \text{K}^{-1}$). Foster et al. (2012) suggested that this range of uncertainty was due to measurement errors and unrealistic assumptions and used a single value of thermal conductivity based on field measurements by Brock et al. (2010). Brock et al. (2010) derived thermal conductivity from glacier melt and debris temperatures and measured a narrower range of thermal conductivity ($0.71\text{--}1.37\text{ W} \cdot \text{m}^{-1} \cdot \text{K}^{-1}$). Future studies should investigate this alternative approach for measuring thermal conductivity and compare these estimates to those of Conway and Rasmussen (2000). This exercise will help determine if the uncertainty associated with the thermal conductivity can be reduced, which would significantly reduce the uncertainty associated with the debris thickness estimates.

The elevation change was the only parameter that showed a clear linear relationship ($R^2 > 0.8$) between debris thickness and the R^2 value for each box (Figure S4). For the thicker debris ($>0.5\text{ m}$) on Ngozumpa and Khumbu Glaciers, the mean R^2 value was 0.35 and 0.31, respectively. This suggests that the uncertainty associated with thicker debris could be reduced by lowering the errors associated with the elevation change estimates, for example, by using DEMs that span a longer period of time. On the other hand, for thinner debris ($<0.5\text{ m}$), the low R^2 values suggest that the debris thickness estimates are not as sensitive to uncertainty in the elevation changes, which is likely because a small change in debris thickness is able to account for any changes in the surface lowering as described in section 5.1.

The same reasoning explains the low R^2 values associated with the flux divergence; that is, the active portion of the glacier that had nonnegligible flux divergences was located further upglacier, where the debris thickness is known to be thinner. Therefore, a small change in debris thickness was able to compensate for changes in the flux divergence. Despite the low R^2 values, the flux divergence is known to have a large impact on the debris thickness estimates. For example, the box located 11.2 km from the terminus of Ngozumpa (Figure 5) had an unrealistically high debris thickness due to the positive flux divergence. Similarly, the box located 8.4 km from the terminus of Khumbu Glacier had an unrealistically high debris thickness (Figure 8) due to the low estimate of flux divergence that resulted from the surface velocities upglacier of this box being poorly resolved (Figure 3). These two examples illustrate that the flux divergence needs to be properly accounted for in order for the MC-Østrem inversion method to produce realistic debris thicknesses.

A sensitivity analysis determined that allowing γ , the ratio of the mean velocity of ice to the surface velocity, to range from 0.8 to 1.0 by assuming a uniform distribution in the Monte Carlo simulations increased the flux divergence estimates by 5–14%. Given the limited impact that small changes in flux divergence has on the debris thickness as described above, variations in γ can be considered minimal. Nonetheless, future work should seek to quantify the influence of basal sliding. Additionally, these simple approaches for estimating flux divergence should be compared to physically based dynamic models and/or field measurements in order to more accurately quantify the uncertainty associated with the flux divergence.

5.4. Additional Sources of Uncertainty

Additional sources of uncertainty include assumptions related to the timing of the melt period and gaps in the meteorological data. We assume that the uncertainty associated with filling in the gaps in the meteorological data is negligible compared to the large sources of uncertainty associated with the debris properties, flux divergence, and elevation change. Regarding the timing of the melt period, the 15 May to 15 October was selected based on existing in situ measurements of the temperature in debris. In the absence of additional information, this is considered a reasonable assumption. The subdebris melt rates at the start and end of the monsoon season are lower than those during the peak of the monsoon, which also suggests that any variations in the start and end dates will not have as large of an impact on the melt rates. Future work should seek to measure the temperature in the debris to quantify the timing of the monsoon more accurately and measure the difference in summer and winter subdebris melt rates.

The last source of uncertainty that should be considered is any factor that influences the accuracy of the elevation change data. These include, but are not limited to, accounting for the snow depth that was on the surface when the DEM was acquired and/or the influence of subglacial drainage system. The 2010 GeoEye-1 stereo image (Table 1) was acquired during the start of the monsoon season in June when meltwater input and routing through and beneath the glacier is at its greatest (Benn et al., 2017). A number of studies have shown that the development of an efficient, channelized subglacial drainage system can cause glacier surface uplift (e.g., Bartholomaus et al., 2011). This process may have led to an increase in surface elevations during the 2010 GeoEye-1 scene acquisition, which would have increased the surface lowering rates compared to later observations.

On the other hand, the 2014 GeoEye-1 stereo image (Table 1) was acquired days after Cyclone Hudhud, which caused the entire glacier and surrounding area to be snow covered. The snow depth at Pyramid Station at this time was ~0.1 m (Figure S2). This snow depth is well within the errors associated with the elevation change, which ranged from 0.2 to 0.5 m. Additionally, no adjustments were made to the 2014 DEM prior to the coregistration, so the coregistration inherently removed the mean snow depth associated with the stable, off-glacier terrain. It is possible that the snow depth was heterogeneous over the glacier, but these variations would be smoothed out when the elevation change estimates were aggregated into boxes. Therefore, the uncertainty associated with the snow depth from Cyclone Hudhud is considered to be minimal. The debris-covered portion of the other DEMs (Table 1) appeared to be free of snow. Ideally snow-free DEMs would be acquired during the same time of year to reduce the errors previously described. Alternatively, a time series of DEMs could be used to estimate the general trend in surface lowering, which would remove any effect that seasonality would have on the elevation change.

5.5. Broader Application

As described in section 5.1, the MC-Østrem inversion method was able to accurately estimate the debris thickness on Ngozumpa, Khumbu, and Imja-Lhotse Shar Glaciers. These accurate estimations of debris thickness are vital for understanding the past, present, and future evolution of debris-covered glaciers. The method's ability to estimate thicker debris (>0.5 m) is particularly important since debris thickness at the terminus of debris-covered glaciers commonly exceeds 0.5 m in the Himalayas (e.g., McCarthy et al., 2017; Ragettli et al., 2015). These areas of thick debris can significantly alter melt rates as the melt associated with 1 m of debris cover is ~50% less than the melt associated with 0.5 m of debris (Figure 10). One of the limiting factors for applying the MC-Østrem inversion method over broader regions is the lack of flux divergence data. The flux divergences were difficult to estimate in areas where the surface velocity may have been poorly resolved (see section 3.3). In these cases, the thermal approach may be a suitable alternative, since the debris thickness in these areas is thinner (<0.5 m) and the thermal approach is not affected by glacier dynamics.

For regional debris thickness estimates, a simplified method may be preferable since the MC-Østrem inversion method requires a series of high-resolution DEMs and meteorological data. Figure 10 shows the relationship between the median debris thickness and the modeled climatic-basal mass balance rate for Ngozumpa, Khumbu, and Imja-Lhotse Shar Glaciers. Despite some variations due to the effects of altitude and topography, there is a strong power law trend ($R^2 = 0.98$). Specifically, the median debris thickness (d) can be estimated from the climatic-basal mass balance rate (\dot{b}) as

$$d = 0.300 \cdot (\dot{b})^{-1.328} \quad (6)$$

The 95% confidence bounds can be used to account for the uncertainty associated with the debris properties as

$$d_{95\%,\text{low}} = 0.125 \cdot (\dot{b})^{-1.157} \quad (7)$$

$$d_{95\%,\text{high}} = 0.699 \cdot (\dot{b})^{-1.431} \quad (8)$$

With these empirical relationships, median debris thickness and the corresponding 95% confidence bounds can be estimated from a pair of DEMs, ice thickness estimates, and surface velocity data. However, the relationship between climatic-basal mass balance rate and debris thickness should be investigated in detail in other regions to determine its broader applicability.

6. Conclusions

We developed a novel method (MC-Østrem inversion) for estimating debris thickness on debris-covered glaciers in the Everest region from elevation change and flux divergence estimates. The method was calibrated and validated for Ngozumpa Glacier using DEMs from 2010 to 2012 and 2012 to 2014. The calibrated debris thickness estimates on Ngozumpa Glacier decreased upglacier and agreed well with existing in situ measurements. The debris thickness estimates were derived by both including and excluding ice cliffs and supraglacial ponds, which found that the mixed box effect can reduce debris thickness by up to 0.8 m over the thickest parts of the glacier. The method was also applied to Khumbu and Imja-Lhotse Shar Glaciers to highlight its regional application.

The comparison of measured and modeled elevation change from 2012 to 2014 on Ngozumpa Glacier showed that the method performed well over both active and stagnant portions of the glacier. The modeled elevation change accounts for the uncertainty associated with the debris thickness estimates, debris properties, and flux divergence, which are much larger than the errors associated with the measured elevation change. The primary source of uncertainty for the calibrated debris thickness estimates was the thermal conductivity.

To the authors' knowledge, this is the first time that debris thickness estimates have been properly validated over an entire glacier using multiple, independent sets of data. The method's ability to accurately estimate thicker debris (>0.5 m) is a major improvement over previous approaches and creates a step-change in our ability to model the past, present, and future evolution of debris-covered glaciers. Future work should assess the performance of the MC-Østrem inversion method in other regions to determine its broader applicability.

Acknowledgments

The authors would like to acknowledge the support of the NSF-CNH program (award 1516912) and the NASA-ROSES program (grant NNX17AB27G) for the support of David Rounce. Michael McCarthy was supported by the NERC DTP (grant NE/L002507/1) and receives CASE funding from Reynolds International Ltd. David Shean was supported by the NASA cryosphere program (award NNX16AQ88G). Special thanks to Matthias Huss for providing the ice thickness data. The meteorological data from Pyramid Station were collected within the SHARE Project thanks to contributions from the Italian National Research Council and the Italian Ministry of Foreign Affairs. The NCEP Reanalysis data were provided by the NOAA/OAR/ESRL PSD, Boulder, Colorado, United States, from their website <http://www.esrl.noaa.gov/psd/>. Model code used in this study are available in online repositories as detailed within the text. Data sets generated in this study, which include debris thickness, flux divergence, box outlines, master DEMs, median x and y horizontal surface velocities, and elevation change for each pair of DEMs for Ngozumpa, Khumbu, and Imja-Lhotse Shar Glaciers, are all available online (<https://doi.org/10.5281/zenodo.1206201>). We would also like to thank Lindsey Nicholson and two anonymous reviewers for their valuable comments on this study.

References

- Bartholomaeus, T. C., Anderson, R. S., & Anderson, S. P. (2011). Growth and collapse of the distributed subglacial hydrologic system of Kennicott Glacier, Alaska, USA, and its effects on basal motion. *Journal of Glaciology*, *57*(206), 985–1002. <https://doi.org/10.3189/002214311798843269>
- Benn, D. I., Thompson, S., Gulle, J., Mertes, J., Luckman, A., & Nicholson, L. (2017). Structure and evolution of the drainage system of a Himalayan debris-covered glacier, and its relationship with patterns of mass loss. *The Cryosphere Discuss.*, 1–43. <https://doi.org/10.5194/tc-2017-29>
- Bolch, T., Buchroithner, M. F., Peters, J., Baessler, M., & Bajracharya, S. (2008). Identification of glacier motion and potentially dangerous glacial lakes in the Mt. Everest region/Nepal using spaceborne imagery. *Natural Hazards and Earth System Sciences*, *8*(6), 1329–1340. <https://doi.org/10.5194/nhess-8-1329-2008>
- Bolch, T., Kulkarni, A., Käbb, A., Huggel, C., Paul, F., Cogley, J. G., et al. (2012). The state and fate of Himalayan Glaciers. *Science*, *336*(6079), 310–314. <https://doi.org/10.1126/science.1215828>
- Bolch, T., Pieczonka, T., & Benn, D. I. (2011). Multi-decadal mass loss of glaciers in the Everest area (Nepal Himalaya) derived from stereo imagery. *The Cryosphere*, *5*(2), 349–358. <https://doi.org/10.5194/tc-5-349-2011>
- Brock, B. W., Mihalcea, C., Kirkbride, M. P., Diolaiuti, G., Cutler, M. E. J., & Smiraglia, C. (2010). Meteorology and surface energy fluxes in the 2005–2007 ablation seasons at the Miage debris-covered glacier, Mont Blanc Massif, Italian Alps. *Journal of Geophysical Research*, *115*, D09106. <https://doi.org/10.1029/2009JD013224>
- Cogley, J. G., Hock, R., Rasmussen, L. A., Arendt, A. A., Bauder, A., Braithwaite, R. J., et al. (2011). Glossary of glacier mass balance and related terms, IHP-VII Technical Documents in Hydrology, No. 86, IACS, Contribution No. 2, UNESCO-IHP, Paris.
- Collier, E., Nicholson, L. I., Brock, B. W., Maussion, F., Essery, R., & Bush, A. B. G. (2014). Representing moisture fluxes and phase changes in glacier debris cover using a reservoir approach. *The Cryosphere*, *8*(4), 1429–1444. <https://doi.org/10.5194/tc-8-1429-2014>
- Conway, H., & Rasmussen, L. A. (2000). Summer temperature profiles within supraglacial debris on Khumbu Glacier, Nepal, Debris-Covered Glaciers, Proceedings of a workshop held at Seattle, Washington, USA, September 2000.
- Dehecq, A., Gourmelen, N., & Trouve, E. (2015). Deriving large-scale glacier velocities from a complete satellite archive: Application to the Pamir-Karakoram-Himalaya. *Remote Sensing of Environment*, *162*, 55–66. <https://doi.org/10.1016/j.rse.2015.01.031>
- Evatt, G. W., Abrahams, D., Heil, M., Mayer, C., Kingslake, J., Mitchell, S. L., et al. (2015). Glacial melt under a porous debris layer. *Journal of Glaciology*, *61*(229), 825–836. <https://doi.org/10.3189/2016JoG14J235>
- Farinotti, D., Brinkerhoff, D. J., Clarke, G. K. C., Fürst, J. J., Frey, H., Gantayat, P., et al. (2017). How accurate are estimates of glacier ice thickness? Results from ITMIX, the Ice Thickness Models Intercomparison experiment. *The Cryosphere*, *11*(2), 949–970. <https://doi.org/10.5194/tc-11-949-2017>
- Farr, T. G., Rosen, P. A., Caro, E., Crippen, R., Duren, R., Hensley, S., et al. (2007). The shuttle radar topography mission. *Reviews of Geophysics*, *45*, RG2004. <https://doi.org/10.1029/2005RG000183>
- Foster, L. A., Brock, B. W., Cutler, M. E. J., & Diotri, F. (2012). Instruments and methods: A physically based method for estimating supraglacial debris thickness from thermal band remote-sensing data. *Journal of Glaciology*, *58*(210), 677–691. <https://doi.org/10.3189/2012JoG11J194>
- Fujita, K., & Sakai, A. (2000). Air temperature environment on the debris-covered area of Lirung Glacier, Langtang Valley, Nepal Himalayas. *International Association of Hydrological Sciences Publication*, *264*, 83–88.
- Fujita, K., Suzuki, R., Nuimura, T., & Sakai, A. (2008). Performance of ASTER and SRTM DEMs, and their potential for assessing glacial lakes in the Lunana region, Bhutan Himalaya. *Journal of Glaciology*, *54*(185), 220–228. <https://doi.org/10.3189/002214308784886162>
- Gades, A., Conway, H., Nereson, N., Naito, N., & Kadota, T. (2000). Radio echo-sounding through supraglacial debris on Lirung and Khumbu Glaciers, Nepal Himalayas. *International Association of Hydrological Sciences Publication*, *264*, 13–22.

- Gardelle, J., Berthier, E., Arnaud, Y., & Käab, A. (2013). Region-wide glacier mass balances over the Pamir-Karakoram-Himalaya during 1999–2011. *The Cryosphere*, 7(4), 1263–1286. <https://doi.org/10.5194/tc-7-1263-2013>
- Höhle, J., & Höhle, M. (2009). Accuracy assessment of digital elevation models by means of robust statistical methods. *ISPRS Journal of Photogrammetry and Remote Sensing*, 64(4), 398–406. <https://doi.org/10.1016/j.isprsjprs.2009.02.003>
- Huss, M., & Farinotti, D. (2012). Distributed ice thickness and volume of all glaciers around the globe. *Journal of Geophysical Research*, 117, F04010. <https://doi.org/10.1029/2012JF002523>
- Immerzeel, W. W., Petersen, L., Ragettli, S., & Pellicciotti, F. (2014). The importance of observed gradients of air temperature and precipitation for modeling runoff from a glacierized watershed in the Nepalese Himalayas. *Water Resources Research*, 50, 2212–2226. <https://doi.org/10.1002/2013WR014506>
- Immerzeel, W. W., van Beek, L. P. H., & Bierkens, M. F. P. (2010). Climate change will affect the Asian water towers. *Science*, 328(5984), 1382–1385. <https://doi.org/10.1126/science.1183188>
- Inoue, J., & Yoshida, M. (1980). Ablation and heat exchange over the Khumbu Glacier. *Seppyo*, 41, 26–31.
- Käab, A., Berthier, E., Nuth, C., Gardelle, J., & Arnaud, Y. (2012). Contrasting patterns of early twenty-first-century glacier mass change in the Himalayas. *Nature*, 488(7412), 495–498. <https://doi.org/10.1038/nature11324>
- Kalnay, E., Kanamitsu, M., Kistler, R., Collins, W., Deaven, D., Gandin, L., et al. (1996). The NCEP/NCAR 40-year reanalysis project. *Bulletin of the American Meteorological Society*, 77(3), 437–471. [https://doi.org/10.1175/1520-0477\(1996\)077<0437:TNYRP>2.0.CO;2](https://doi.org/10.1175/1520-0477(1996)077<0437:TNYRP>2.0.CO;2)
- Kayastha, R. B., Takeuchi, Y., Nakawo, M., & Ageta, Y. (2000). Practical prediction of ice melting beneath various thickness of debris cover on Khumbu Glacier, Nepal, using a positive degree-day factor. *International Association of Hydrological Sciences Publication*, 264, 71–81.
- King, O., Quincey, D. J., Carrivick, J. L., & Rowan, A. V. (2017). Spatial variability in mass loss of glaciers in the Everest region, central Himalayas, between 2000 and 2015. *The Cryosphere*, 11(1), 407–426. <https://doi.org/10.5194/tc-11-407-2017>
- LeJeune, Y., Bertrand, J., Wagnon, P., & Morin, S. (2013). A physically based model of the year-round surface energy and mass balance of debris-covered glaciers. *Journal of Glaciology*, 59(214), 327–344. <https://doi.org/10.3189/2013JoG12J149>
- Mattson, L. E., Gardner, J. S., & Young, G. J. (1993). Ablation on debris covered glaciers: An example from the Rakhiot Glacier, Punjab, Himalaya, Snow and Glacier Hydrology. *International Association of Hydrological Sciences Publication*, 218, 289–296.
- McCarthy, M., Pritchard, H., Willis, I., & King, E. (2017). Ground-penetrating radar measurements of debris thickness on Lirung Glacier, Nepal. *Journal of Glaciology*, 63(239), 543–555. <https://doi.org/10.1017/jog.2017.18>
- Mihalcea, C., Brock, B. W., Diolaiuti, G., D'Agata, C., Citterio, M., Kirkbridge, M. P., et al. (2008). Using ASTER satellite and ground-based surface temperature measurements to derive supraglacial debris cover and thickness patterns on Miage Glacier (Mont Blanc Massif, Italy). *Cold Regions Science and Technology*, 52, 341–354. <https://doi.org/10.1016/j.coldregions.2007.03.004>
- Miles, E., Willis, I., Arnold, N., Steiner, J., & Pellicciotti, F. (2017). Spatial, seasonal and interannual variability of supraglacial ponds in the Langtang Valley of Nepal, 1999–2013. *Journal of Glaciology*, 63(237), 88–105. <https://doi.org/10.1017/jog.2016.120>
- Nakawo, M., Iwata, S., Watanabe, O., & Yoshida, M. (1986). Processes which distribute supraglacial debris on the Khumbu Glacier, Nepal Himalaya. *Annals of Glaciology*, 8, 129–131. <https://doi.org/10.1017/S0260305500001294>
- Nicholson, L. (2004). *Modelling melt beneath supraglacial debris: implications for the climatic response of debris-covered glaciers*, (PhD thesis). University of St Andrews.
- Nicholson, L., & Benn, D. I. (2006). Calculating ice melt beneath a debris layer using meteorological data. *Journal of Glaciology*, 52(178), 463–470. <https://doi.org/10.3189/172756506781828584>
- Nicholson, L., & Benn, D. I. (2012). Properties of natural supraglacial debris in relation to modelling sub-debris ice ablation. *Earth Surface Processes and Landforms*, 38(5), 490–501. <https://doi.org/10.1002/esp.3299>
- Nicholson, L., & Mertes, J. (2017). Thickness estimation of supraglacial debris above ice cliff exposures using a high-resolution digital surface model derived from terrestrial photography. *Journal of Glaciology*, 63(242), 989–998. <https://doi.org/10.1017/jog.2017.68>
- Nuimura, T., Fujita, K., Fukui, K., Asahi, K., Aryal, R., & Ageta, Y. (2011). Temporal changes in elevation of the debris-covered ablation area of Khumbu Glacier in the Nepal Himalaya since 1978. *Arctic, Antarctic, and Alpine Research*, 43(2), 246–255. <https://doi.org/10.1657/1938-4246-43.2.246>
- Nuimura, T., Fujita, K., Yamaguchi, S., & Sharma, R. R. (2012). Elevation changes of glaciers revealed by multitemporal digital elevation models calibrated by GPS survey in the Khumbu region, Nepal Himalaya, 1992–2008. *Journal of Glaciology*, 58(210), 648–656. <https://doi.org/10.3189/2012JoG11J061>
- Nuth, C., & Käab, A. (2011). Co-registration and bias corrections of satellite elevation data sets for quantifying glacier thickness change. *The Cryosphere*, 5(1), 271–290. <https://doi.org/10.5194/tc-5-271-2011>
- Østrem, G. (1959). Ice melting under a thin layer of moraine, and the existence of ice cores in moraine ridges. *Geografiska Annaler*, 41(4), 228–230. <https://doi.org/10.1080/20014422.1959.11907953>
- Patel, L. K., Sharma, P., Thamban, M., Singh, A., & Ravindra, R. (2016). Debris control on glacier thinning—A case study of the Batal glacier, Chandra basin, Western Himalaya. *Arabian Journal of Geosciences*, 9(4), 1–8. <https://doi.org/10.1007/s12517-016-2362-5>
- Pritchard, H. D. (2017). Asia's glaciers are a regionally important buffer against drought. *Nature*, 545(7653), 169–174. <https://doi.org/10.1038/nature22062>
- Quincey, D. J., Luckman, A., & Benn, D. (2009). Quantification of Everest region glacier velocities between 1992 and 2002, using satellite radar interferometry and feature tracking. *Journal of Glaciology*, 55(192), 596–606. <https://doi.org/10.3189/002214309789470987>
- Quincey, D. J., Smith, M. W., Rounce, D. R., Ross, A. N., King, O., & Watson, C. S. (2017). Evaluating morphological estimates of the aerodynamic roughness of debris covered glacier ice. *Earth Surface Processes and Landforms*, 42, 2541–2553. <https://doi.org/10.1002/esp.4198>
- Ragettli, S., Bolch, T., & Pellicciotti, F. (2016). Heterogeneous glacier thinning patterns over the last 40 years in Langtang Himal, Nepal. *The Cryosphere*, 10(5), 2075–2097. <https://doi.org/10.5194/tc-10-2075-2016>
- Ragettli, S., Pellicciotti, F., Immerzeel, W. W., Miles, E. S., Petersen, L., Heynen, M., et al. (2015). Unraveling the hydrology of a Himalayan catchment through integration of high resolution in situ data and remote sensing with an advanced simulation model. *Advances in Water Resources*, 78, 94–111. <https://doi.org/10.1016/j.advwatres.2015.01.013>
- Reid, T. D., & Brock, B. W. (2010). An energy-balance model for debris-covered glaciers including heat conduction through the debris layer. *Journal of Glaciology*, 56(199), 903–916. <https://doi.org/10.3189/002214310794457218>
- Reid, T. D., Carenzo, M., Pellicciotti, F., & Brock, B. W. (2012). Including debris cover effects in a distributed model of glacier ablation. *Journal of Geophysical Research*, 117, D18105. <https://doi.org/10.1029/2012JD017795>
- Rounce, D. R., & McKinney, D. C. (2014). Debris thickness of glaciers in the Everest area (Nepal Himalaya) derived from satellite imagery using a nonlinear energy balance model. *The Cryosphere*, 8(4), 1317–1329. <https://doi.org/10.5194/tc-8-1317-2014>
- Rounce, D. R., Quincey, D. J., & McKinney, D. C. (2015). Debris-covered glacier energy balance model for Imja-Lhotse Shar Glacier in the Everest region of Nepal. *The Cryosphere*, 9(6), 2295–2310. <https://doi.org/10.5194/tc-9-2295-2015>

- Rowan, A. V., Egholm, D. L., Quincey, D. J., & Glasser, N. F. (2015). Modelling the feedbacks between mass balance, ice flow and debris transport to predict the response to climate change of debris-covered glaciers in the Himalaya. *Earth and Planetary Science Letters*, *430*, 427–438. <https://doi.org/10.1016/j.epsl.2015.09.004>
- Salerno, F., Guyennon, N., Thakuri, S., Viviano, G., Romano, E., Vuillermoz, E., et al. (2015). Weak precipitation, warm winters and springs impact glaciers of south slopes of Mt. Everest (central Himalaya) in the last 2 decades (1994–2013). *The Cryosphere*, *9*(3), 1229–1247. <https://doi.org/10.5194/tc-9-1229-2015>
- Salerno, F., Thakuri, S., Tartari, G., Nuimura, T., Sunako, S., Sakai, A., & Fujita, K. (2017). Debris-covered glacier anomaly? Morphological factors controlling changes in the mass balance, surface area, terminus position, and snow line altitude of Himalayan glaciers. *Earth and Planetary Science Letters*, *471*, 19–31. <https://doi.org/10.1016/j.epsl.2017.04.039>
- Schauwecker, S., Rohrer, M., Huggel, C., Kulkarni, A., Ramanathan, A., Salzmann, N., et al. (2015). Remotely sensed debris thickness mapping of Bara Shigri Glacier, Indian Himalaya. *Journal of Glaciology*, *61*(228), 675–688. <https://doi.org/10.3189/2015/JoG14J102>
- Shea, J. M., Immerzeel, W. W., Wagnon, P., Vincent, C., & Bajracharya, S. (2015). Modelling glacier change in the Everest region, Nepal Himalaya. *The Cryosphere*, *9*(3), 1105–1128. <https://doi.org/10.5194/tc-9-1105-2015>
- Shean, D. (2017a). High mountain Asia 8-meter DEMs derived from along-track optical imagery, Version 1. Boulder, CO: NASA National Snow and Ice Data Center Distributed Active Archive Center. <https://doi.org/10.5067/GSACB044M4PK>
- Shean, D. (2017b). High mountain Asia 8-meter DEMs derived from cross-track optical imagery, Version 1. Boulder, CO: NASA National Snow and Ice Data Center Distributed Active Archive Center. <https://doi.org/10.5067/0MCWJH5ABYO>
- Shean, D. E., Alexandrov, O., Moratto, Z. M., Smith, B. E., Joughin, I. R., Porter, C., & Morin, P. (2016). An automated, open-source pipeline for mass production of digital elevation models (DEMs) from very-high-resolution commercial stereo satellite imagery. *ISPRS Journal of Photogrammetry*, *116*, 101–117. <https://doi.org/10.1016/j.isprsjprs.2016.03.012>
- Somos-Valenzuela, M. A., McKinney, D. C., Rounce, D. R., & Byers, A. C. (2014). Changes in Imja Tsho in the Mount Everest region of Nepal. *The Cryosphere*, *8*(5), 1661–1671. <https://doi.org/10.5194/tc-8-1661-2014>
- Soncini, A., Bocchiola, D., Confortola, G., Minora, U., Vuillermoz, E., Salerno, F., et al. (2016). Future hydrological regimes and glacier cover in the Everest region: The case study of the upper Dudh Koshi basin. *Science of the Total Environment*, *565*, 1084–1101. <https://doi.org/10.1016/j.scitotenv.2016.05.138>
- Takeuchi, Y., Kayastha, R. B., & Nakawo, M. (2000). Characteristics of ablation and heat balance in debris-free and debris-covered areas on Khumbu Glacier, Nepal Himalayas. In *The pre-monsoon season, Int. Assoc. Hydrol. Sci. Publ.* (Vol. 264, pp. 53–61).
- Thakuri, S., Salerno, F., Bolch, T., Guyennon, N., & Tartari, G. (2016). Factors controlling the accelerated expansion of Imja Lake, Mount Everest region, Nepal. *Annals of Glaciology*, *57*(71), 245–257. <https://doi.org/10.3189/2016AoGA063>
- Thakuri, S., Salerno, F., Smiraglia, C., Bolch, T., D'Agata, C., Viviano, G., & Tartari, G. (2014). Tracing glacier changes since the 1960s on the south slope of Mt. Everest (central Southern Himalaya) using optical satellite imagery. *The Cryosphere*, *8*(4), 1297–1315. <https://doi.org/10.5194/tc-8-1297-2014>
- Thompson, S., Benn, D. I., Mertes, J., & Luckman, A. (2016). Stagnation and mass loss on a Himalayan debris-covered glacier: Processes, patterns and rates. *Journal of Glaciology*, *62*(233), 467–485. <https://doi.org/10.1017/jog.2016.37>
- Thompson, S. S., Benn, D. I., Dennis, K., & Luckman, A. (2012). A rapidly growing moraine-dammed glacial lake on Ngozumpa Glacier, Nepal. *Geomorphology*, *145–146*, 1–11. <https://doi.org/10.1016/j.geomorph.2011.08.015>
- Vincent, C., Wagnon, P., Shea, J. M., Immerzeel, W. W., Kraaijenbrink, P., Shrestha, D., et al. (2016). Reduced melt on debris-covered glaciers: Investigations from Changri Nup Glacier, Nepal. *The Cryosphere*, *10*(4), 1845–1858. <https://doi.org/10.5194/tc-10-1845-2016>
- Watson, C. S., Quincey, D. J., Carrivick, J. L., & Smith, M. W. (2016). The dynamics of supraglacial ponds in the Everest region, central Himalaya. *Global and Planetary Change*, *142*, 14–27. <https://doi.org/10.1016/j.gloplacha.2016.04.008>
- Watson, C. S., Quincey, D. J., Carrivick, J. L., & Smith, M. W. (2017). Ice cliff dynamics in the Everest region of the Central Himalaya. *Geomorphology*, *278*(1), 238–251. <https://doi.org/10.1016/j.geomorph.2016.11.017>
- Wu, Z., & Liu, S. (2012). Imaging the debris internal structure and estimating the effect of debris layer on ablation of glacier ice. *Journal of the Geological Society of India*, *80*(6), 825–835. <https://doi.org/10.1007/s12594-012-0211-z>